SEDIMENTOLOGY the journal of the International Association of Sedimentologists

Sedimentology (2015) **62**, 1360–1383 doi: 10.1111/sed.12186

Depositional system and palaeoclimatic interpretations of Middle to Late Pleistocene travertines: Kocabaş, Denizli, south-west Turkey

EZHER TOKER*, MINE SEZGÜL KAYSERI-ÖZER†, MEHMET ÖZKUL* and SÁNDOR KELE‡§

**Department of Geological Engineering, Pamukkale University, Kınıklı, TR-20070 Denizli, Turkey (E-mail: egulbas@pau.edu.tr)*

†Institute of Marine Science and Technology, Dokuz Eylul University, Haydar Aliyev Bul. No: 100, 35430 İnciraltı-İzmir, Turkey

‡Geological Institute, ETH Zurich, Sonneggstrasse 5, 8092 Zürich, Switzerland

§Institute for Geological and Geochemical Research, Research Centre for Astronomy and Earth Sciences, Hungarian Academy of Sciences, H-1112 Budapest, Budaörsi u. 45, Hungary

Associate Editor – Daniel Ariztegui

ABSTRACT

Travertine deposits in western Turkey are very well-exposed in the area of Kocabaş, in the eastern part of the Denizli Basin. The palaeoclimatic significance of these travertines is discussed using U/Th dates, stable isotope data and palynological evidence. The Kocabaş travertine occurrences are characterized by successions of depositional terraces associated with palaeosols and karstic features. The travertines have been classified into eight lithotypes and one erosional horizon, namely: laminated, coated bubble, reed, paper-thin raft, intraclasts, micritic travertine with gastropods, extra-formational pebbles and a palaeosol layer. The analysed travertines mostly formed between 181 ka and 80 ka (Middle to Late Pleistocene) during a series of climatic changes including glacial and interglacial intervals; their $\delta^{13}C$ and $\delta^{18}O$ values indicate that the depositional waters were mainly of basinal thermal origin, occasionally mixed with surficial meteoric water. Palynological results obtained from the palaeosols showed an abundance of non-arboreal percentage and xerophytic plants (Oleaceae and *Quercus* evergreen type) indicating that a drought occurred. Marine Isotope Stage 6 is represented by grassland species but Marine Isotope Stage 5 is represented by Pinaceae–*Pinus* and *Abies*, *Quercus* and Oleaceae. Uranium/thorium analyses of the Kocabaş travertines show that deposition began in Marine Isotope Stage 6 (glacial) and continued to Marine Isotope Stage 4 (glacial), but mostly occurred in Marine Isotope Stage 5 (interglacial). The travertine deposition continued to *ca* 80 ka in the south-west of the study area, in one particular depression depositional system. Palaeoenvironmental indicators suggest that the travertine depositional evolution was probably controlled by fault-related movements that influenced groundwater flow. Good correlation of the stable isotope values and dates of deposition of the travertines and palynological data of palaeosols in the Kocabaş travertines serve as a starting point for further palaeoclimate studies in south-west Turkey. Additionally, the study can be compared with other regional palaeoclimate archives.

Keywords Dating, Middle to Late Pleistocene, palaeoclimate, palaeoenvironmental evolution, pollen analysis, stable isotopes, SW Turkey, travertine lithotypes.

INTRODUCTION

Travertines, tufas and speleothems are environmental, hydrological, tectonic and climatological archives of the time span in which they formed (Andrews *et al.*, 1997; Bar-Matthews *et al.*, 1997; Hancock *et al.*, 1999; Minissale *et al.*, 2002; Andrews, 2006; Pedley, 2009; De Flippis *et al.*, 2012; Gandin & Capezzuoli, 2014). To date, tufas and speleothems have been preferred to travertines for palaeoenvironmental and palaeoclimatic reconstructions (Boch *et al.*, 2005; Andrews, 2006; Fairchild *et al.*, 2006; Arenas *et al.*, 2007, 2010; Bertini *et al.*, 2007, 2008, 2014), mainly because stable isotopes in travertines are less predictable in terms of disequilibrium effects. For example, the $\delta^{13}C$ values of tufas and speleothems are influenced mostly by organic and atmospheric sources while the $\delta^{13}C$ values of travertines are governed mainly by thermal sources and the dissolution of basinal carbonates (Chafetz & Folk, 1984; Folk, 1993; Horvatincic *et al.*, 2005; Pentecost, 2005; Andrews, 2006).

Nevertheless, Late Pleistocene travertines near Rapolano Terme and Serre di Rapolano in Tuscany, central Italy, have been characterized by their facies and depositional system types by Guo & Riding (1998). Hot spring travertines were grouped into three depositional systems: Slope Depositional System, Depression Depositional System and Reed Mound Depositional System. Slope Systems were further disaggregated into 'Terrace Slope Facies', 'Smooth Slope Facies' and 'Waterfall Facies'. In the same manner, Depression Depositional Systems (cf. 'shallow lake-fill deposits' of Chafetz & Folk, 1984) were subdivided into 'Shrub-Flat Facies' (including laminae and gas bubbles) and 'Marsh-Pool Facies' (formed mainly of intraclasts and reeds; Guo & Riding, 1998; Özkul *et al.*, 2002; Gandin & Capezzuoli, 2014). Furthermore, the close relationships between travertine deposition and tectonic activity, including faulting, was established for Middle to Late Pleistocene travertines of the Northern Apennines (Brogi & Capezzuoli, 2009), while Altunel & Hancock (1993b) and Altunel (1994) described in fissure ridge travertines and detailed neotectonic structures within and cutting the Pamukkale travertines of the Denizli Basin. Van Noten *et al.* (2013) also inferred the different local palaeostress directions that are activated after travertine deposition to understand the neotectonic activity in the Denizli Basin, Turkey. Despite all related studies on the travertine and tufa systems in several outcrops all around the world, there are still some gaps in understanding, such as a deficiency of detailed sedimentological analyses, stable isotopes, palynological data and dating results. Firstly in this study, responses of these methods were determined, and also palaeoclimatic conditions of the region were elucidated by using the correlated data.

This article focuses on travertine occurrences, located in the Kocabaş area in the eastern part of Denizli, south-west Turkey (Fig. 1), where different types of travertine precipitation can be seen clearly. This research shows that these precipitates and their sedimentation rate were probably controlled by palaeoclimatic conditions and tectonic activity of the region during the Quaternary period. The purpose of this study was to reconstruct the palaeoenvironmental and palaeoclimatic evolution of the Kocabaş travertines. Thus, it can be correlated with other travertine precipitations, in particular all Mediterranean travertine and tufa systems during the Middle to Late Pleistocene.

GEOLOGICAL SETTING

The Denizli Basin, located in the western Anatolian Extensional Province of Turkey, is a graben bounded by normal faults along its northern and southern margins (Koçyiğit, 2005; Westaway *et al.*, 2005; Kaymakçı, 2006; Fig. 1). The basin includes the world famous Pamukkale travertines and, due to regional tectonic activity along the north-west trended Pamukkale Fault zone, the Denizli half graben became a full graben (Altunel & Hancock, 1993a; Çakır, 1999; Şimşek *et al.*, 2000; Özkul *et al.*, 2002; Alçiçek *et al.*, 2007; Kele *et al.*, 2011; De Flippis *et al.*, 2012; Özkul *et al.*, 2013; Van Noten *et al.*, 2013).

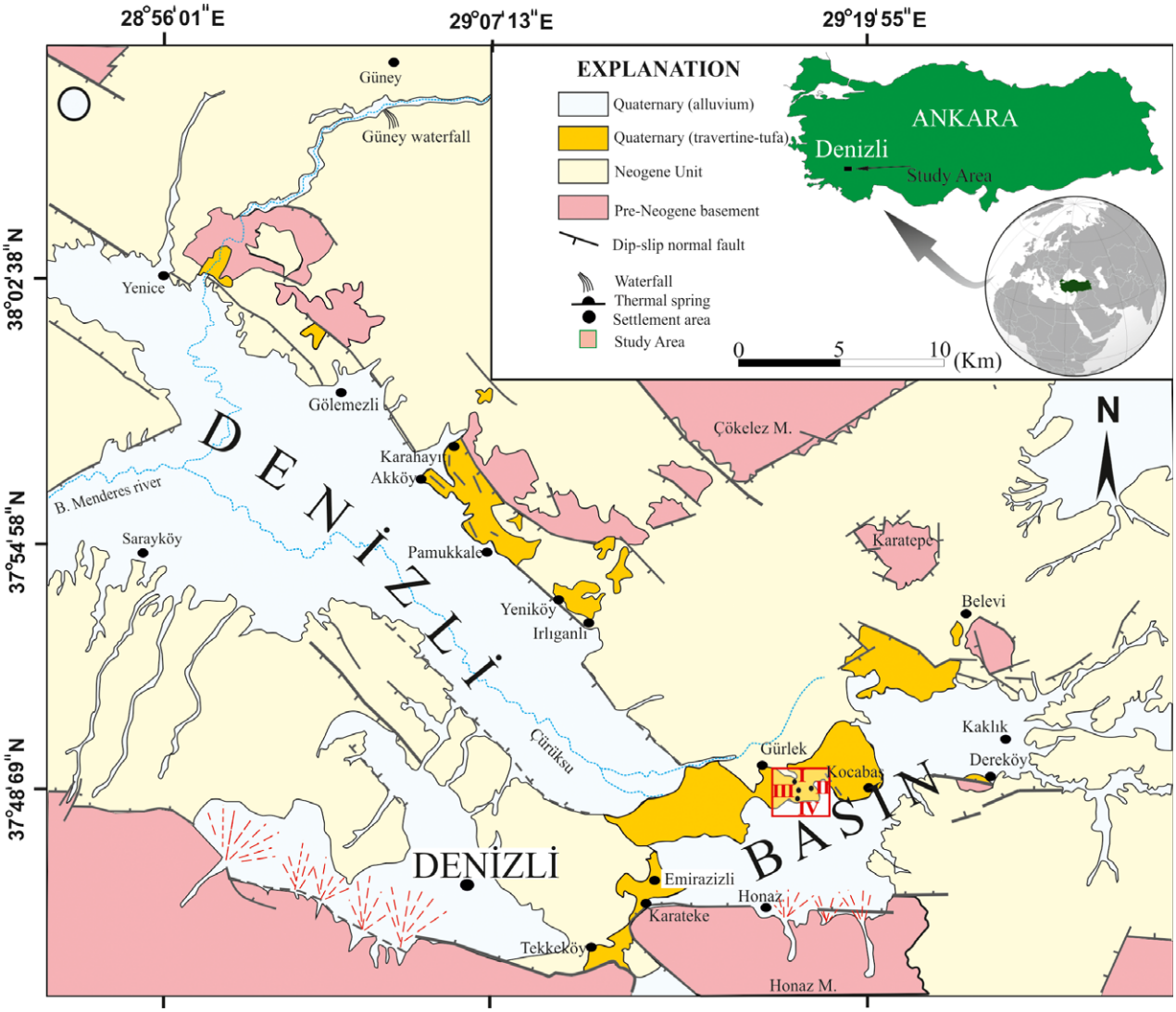

Fig. 1. Base map showing the location of the study area and travertine quarries. (A) Location of the Denizli area in SW Turkey and geological map of the studied area (after Sun, 1990; Özkul *et al.*, 2002). (B) Simplified geological map of the Denizli Basin showing part of the travertine sites (I, II, III and IV) between the Kocabaş and Gürlek settlements.

The travertine deposits overlie Neogene basin fill of alluvial, fluvial and lacustrine deposits. The basin began as a half graben in the upper Early Miocene when deposition gradually evolved from alluvial to fluvial and finally into lacustrine towards the Gelasian (Westaway, 1993; Alçiçek *et al.*, 2007); older bedrocks are exposed on the graben shoulders and in the mountainous areas (Özkul *et al.*, 2002, 2013). The bedrock mostly consists of schists and marbles that form the Menderes Massif (Bozkurt & Oberhänsli, 2001; Erdoğan & Güngör, 2004) and the allochthonous Mesozoic limestone, dolomite and gypsum of the Lycian Nappes that tectonically overlay the Menderes Massif (Okay, 1989; Sözbilir, 1997, 2005; Gündoğan *et al.*, 2008). Travertine precipitation is represented by local fluvial terraces that become progressively younger towards the basin centre (Koçyiğit, 2005; Kaymakçı, 2006; Kazancı *et al.*, 2012). The Quaternary faults and fissures in the carbonate bedrocks along the graben margins are natural pathways for the descending meteoric waters and upwelling of hydrothermal fluids to the surface (Altunel & Hancock, 1993a,b; Minissale *et al.*, 2002; Dilsiz, 2006; Brogi & Capezzuoli, 2009; Özkul *et al.*, 2013).

The investigated area includes the Kocabaş site that is located in the north-eastern part of the Denizli Basin. This area is characterized by

travertine occurrences such as the Kaklik and Pamukkale (Fig. 1). The travertines of Kocabaş and surrounding areas are mostly vertically banded travertines (centre of fissure ridges) and horizontally and subhorizontally bedded travertines precipitated in adjacent pools or shallow lake environments (Özkul *et al.*, 2002; Altunel & Karacabak, 2005; De Flippis *et al.*, 2012; Özkul *et al.*, 2013, 2014). The fissure ridges frequently occur along the north-west margin of the basin and most probably developed at the ends of the normal fault segments or step-over zones between them (Çakır, 1999; Brogi *et al.*, 2014).

MATERIALS AND METHODS

Sixty travertine samples were collected for stable carbon and oxygen isotope analyses, 13 samples were collected for U/Th dating and 76 travertine and muddy–silty samples were collected for palynological investigations. During the field study, sedimentological observations were conducted in order to determine the different travertine lithotypes and facies of the travertine depositional system. Both the geographic position and elevation of the travertines were measured using GPS.

Stable isotope analysis

The stable isotope analyses were performed on 60 travertine samples at the Institute for Geological and Geochemical Research, Hungarian Academy of Sciences, Budapest, Hungary. Carbon and oxygen isotope analyses of bulk carbonate samples were carried out using continuous flow technique (Spötl & Vennemann, 2003). The $^{13}C/^{12}C$ and $^{18}O/^{16}O$ ratios were determined in CO_2 gases liberated by phosphoric acid using a Finnigan delta plus XP mass spectrometer (Thermo Fisher Scientific, Bath, UK). Standardization was conducted using laboratory calcite standards calibrated against National Bureau of Standards (NBS) 18 and NBS 19. All samples were measured at least in duplicate and the mean values are expressed in the conventional δ notation in parts per thousand (‰) on the Vienna Pee Dee Belemnite (VPDB) scale ($\delta^{13}C$, $\delta^{18}O$) and Vienna Standard Mean Ocean Water (VSMOW) scale ($\delta^{18}O$). Reproducibilities are better than ±0·1‰ for $\delta^{13}C$ and $\delta^{18}O$ values of carbonates.

Uranium/thorium dating

Uranium-series dating of travertine samples was carried out at the GEOTOP research centre of the University of Quebec at Montreal. Travertine samples, each weighing a few grams, were cut using a Dremel® rotary tool (Robert Bosch Tool Corporation, Mount Prospect, IL, USA). The external layer of the sample was removed in order to reduce the risk of contamination by ^{230}Th-bearing detrital particles. The travertine sample was then heated in a clean crucible in order to destroy organic matter and was then further dissolved with a 7 N HNO_3 in Teflon® beakers. A known amount of spike (^{233}U, ^{236}U and ^{229}Th) was added to determine U and Th isotopes using the isotope dilution technique.

The U–Th separation was conducted using an AG1X8 anionic resin bed. The Th and U–Fe fractions were retrieved by elution with 6 N HCl and H_2O, respectively. The purification of the U fraction was accomplished using 0·2 ml U-Teva (Eichrom® Industries; Darien, IL, USA) resin volume. The U–Fe separation was performed by elution using 3 N HNO_3 (Fe fraction) and 0·002 N HNO_3 (U fraction). The overall analytical reproducibility, as estimated from replicate measurements of standards, is usually better than 0·5% for U concentration and $^{234}U/^{238}U$ ratios, and ranges from 0·5 to 1% for $^{230}Th/^{234}U$ ratios (2 sigma error ranges).

Despite the mechanical abrasion, some detrital fraction remained as indicated by the presence of ^{232}Th. This remaining fraction indicates that a part of the measured ^{230}Th is related to a detrital contamination that has been added to the ^{230}Th produced by the authigenic uranium of the $CaCO_3$. In order to account for the ^{230}Th related to the detrital fraction, a correction was carried out according to Ludwig & Paces (2002). Specifically, ^{232}Th was used as an index and a typical crustal Th/U ratio was assumed, with $^{234}U/^{238}U$ and $^{230}Th/^{238}U$ activity ratios near secular equilibrium. In this model, the isotope and the activity ratios used were $(^{232}Th/^{238}U) = 1{\cdot}21 \pm 50\%$, $(^{234}U/^{238}U) = 1 \pm 10\%$ and $(^{230}Th/^{238}U) = 1 \pm 10\%$.

Palynological analysis

Seventy-six samples were collected for pollen analyses, 47 samples from terrestrial carbonates and 29 from palaeosol levels (Fig. 1B). Pollen

samples were treated with hydrogen chloride (HCl), hydrogen fluoride (HF) and potassium hydroxide (KOH) following standard procedures (Kaiser & Asraf, 1974). The residue was sieved with a mesh–size of 10 μm. Only 29 samples collected from the palaeosol levels in Sites I, II and IV were suitable for qualitative and quantitative pollen analysis. Approximately 150 individual palynomorphs (pollen and dinocysts) per sample were counted. Palynomorph identification was performed under an Olympus light microscope (Olympus Corporation, Tokyo, Japan), usually at 100×, 40× and 20× magnifications. The palynomorph diagram was prepared with a Tilia graph (2·0).

RESULTS

Travertine lithotypes

Eight different lithotypes, most of them previously described in many travertine sites (Chafetz & Folk, 1984; Guo & Riding, 1998; Özkul *et al.*, 2002; Brogi & Capezzuoli, 2009), have been observed and interpreted based on their depositional features (for example, colour, bedding, lamination and fossil content) along the measured sections from four travertine quarry walls (Fig. 1). The following main travertine lithotypes are recognized (Fig. 2): (i) Laminated (L1); (ii) Coated bubble (L2); (iii) Reed (L3); (iv) Paper-thin raft (L4); (v) Intraclast (L5); (vi) Micritic travertine with gastropods (L6); and (vii) Extra-formational pebbles (L7). An additional lithotype, palaeosol bed (L8), was mapped and described, as representing an accumulation of alluvial deposits by erosion when travertine deposition ceased. The different travertine lithotypes in the study area are described below in detail.

Laminated travertine (L1)

This lithotype, up to 50 cm thick, is white to light brown in colour with dense tabular micritic laminae. The latter are parallel, with horizontal or, more commonly, slightly undulatory profiles. Some planar pores parallel to laminations also occur. Individual lamina thickness varies between 0·3 mm and 2 mm. Laminae have transitional boundaries and are characterized by variations in colour. The density of the lamination has most probably been caused by seasonal changes and by algal filaments. The whitish layers may have precipitated mainly inorganically, while the dark layers correspond to the incorporation of organic components. The dark laminae are porous while the whitish laminae are less porous, and more dense and compact. This lithotype is present in all travertine sections of the study area, and is overlain by the reed lithotypes composed of plant clusters (Figs 2B and 3).

Coated bubble travertine (L2)

This lithotype is characterized by coated gas bubbles in relation to paper-thin raft and reed lithotypes (Fig. 2C). Carbonate-encrusted bubbles were first described by Allen & Day (1935) and subsequently mentioned by many authors (e.g. Kitano, 1963; Schreiber *et al.*, 1981; Chafetz & Folk, 1984). Coated bubble has also been referred to as 'lithified bubble' and 'foam rock' by Guo & Riding (1998); Jones & Renaut (2010); Chafetz & Folk (1984). In addition, Guo & Riding (1998) pointed out that individual bubbles at Rapolano Terme are observed as tube-shaped, aligned in a vertical chain; however, the shape of the bubbles in the Kocabaş sections are mainly spherical and oblate and their size ranges from millimetre to centimetre. This lithotype has been detected in the lower middle portion of the measured section.

Fig. 2. View of Kocabaş travertine quarries deposited in a Depressional Depositional System and showing in detail its lithotype features. (A) One of the travertine quarries showed some lithotypes (L1, L3, L5 and L8) (scale: 178 cm). (B) Horizontally bedded, parallel laminated travertine (pl) is clearly seen between palaeosol layer (p) on top and clast breccias (br) (scale is 170 cm). (C) Gas bubbles (gb) in Flat-Pool facies; the horizontal lamination is accentuated (black line; scale: 12 cm). (D) Vertical and encrusted moulds of stems (reed travertine) intercalated with gas bubbles. (E) Angular and subangular travertine fragments called intraclasts (travertine breccias-br) are a common lithotype in Marsh-Pool facies. The hammer is 32·5 cm long; (F) Gastropods (gs) are locally common in Marsh-Pool facies and are clearly visible in detritic levels of travertine deposits. The coin is 2·5 cm in diameter. (G) Unconformity between two travertine bodies which are highlighted by a palaeosol (p) and intense alteration (erosional surface). (H) Extra-formational pebbles with rounded shape are observed at the margin of the travertine deposits. (I) Microscope image, gastropod shell surrounded by micritic cement in thin section. (J) Microscope image shows two ostracod (o) fragments surrounded by micritic cement with the inside filled by spar calcite.

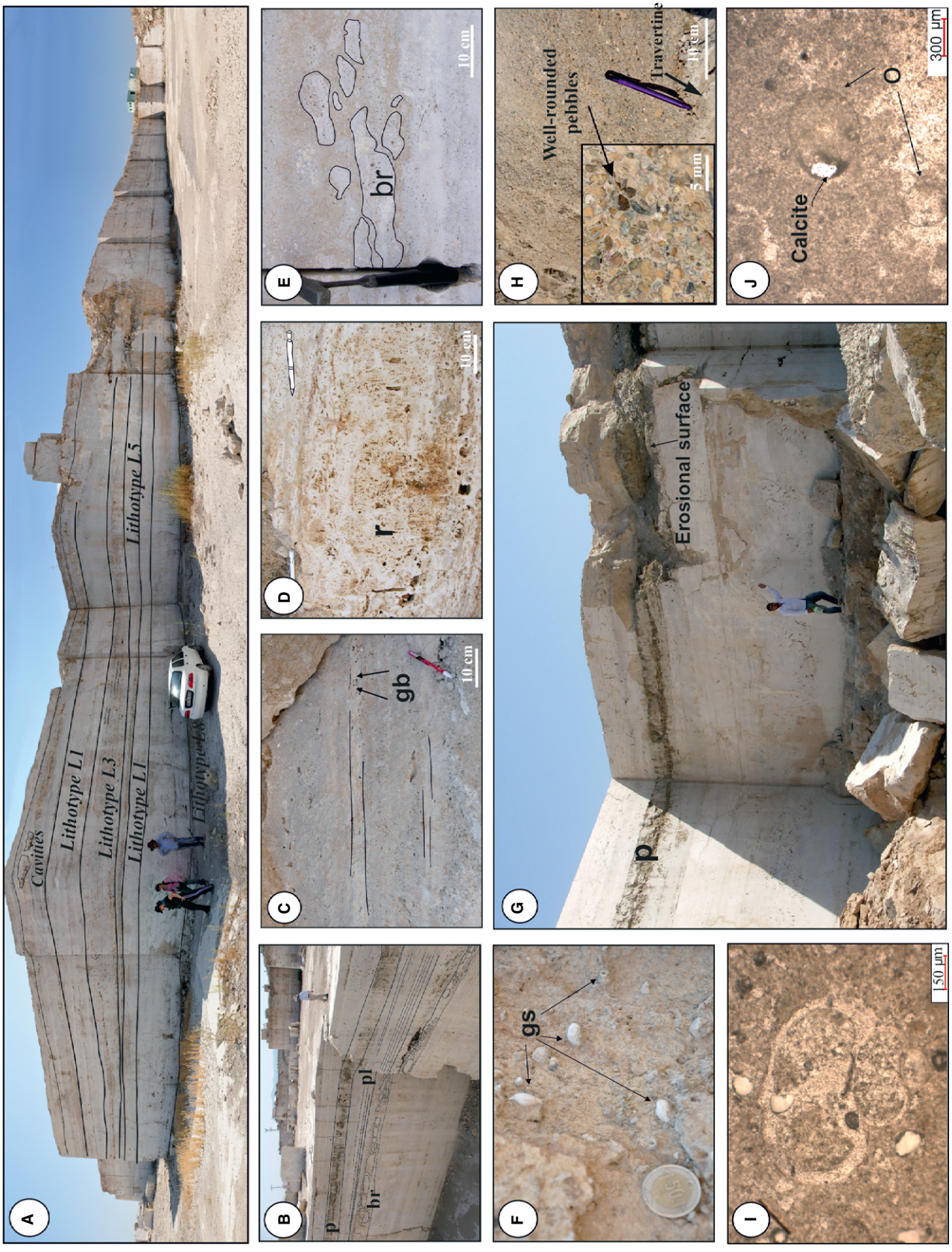
A
Cavities
Lithotype L1
Lithotype L3
Lithotype L1
Lithotype L5
Lithotype L6
B
p
br
pl
C
gb
10 cm
D
r
10 cm
E
br
10 cm
F
gs
5p
G
Erosional surface
p
H
Well-rounded pebbles
Travertine
5 mm
10 cm
I
150 µm
J
Calcite
O
300 µm

Reed travertine (L3)
This lithotype is recognized as vertically oriented and encrusted moulds of stems occasionally intercalated with coated bubbles. Its approximate thickness is up to 3 to 4 m and laterally continues for several hundred metres (Figs 2D and 3). This lithotype is mostly in the middle portion of all sections.

Paper-thin rafts (L4)
Calcite or aragonite rafts develop at the water surface of stagnant pools where surface degassing of CO_2 increases the saturation level, leading to calcite or aragonite precipitation (Folk *et al.*, 1985; Chafetz *et al.*, 1991; Capezzuoli & Gandin, 2005; Jones & Renaut, 2010). The lithotype is composed of few thin individual millimetre thick sheets and accompanied by coated bubbles and reed lithofacies (Figs 2 and 3). This lithofacies is described as 'paper-thin raft' (Guo & Riding, 1998), 'hot water ice' (Allen & Day, 1935), 'calcite ice' (Bargar, 1978) and 'calcite rafts' (Folk *et al.*, 1985) in hot spring environments and in cool water cave pools (Baker & Frostick, 1951; Black, 1953). The colours of rafts range from beige to light brown based on the chemical composition of the water. This lithotype is generally observed mostly in the middle portion of all sections.

Intraclast travertine (L5)
Generally, coeval erosion and breakage of travertine produce abundant lithoclasts. Such erosion typically occurs during periods of increased flow rates that might be caused by a periodic surge in the spring flow rates or flooding after periods of heavy rain. Detritus produced in this manner is washed downslope, and accumulates in depressions or pond areas (e.g. Guo & Riding, 1998; Sant'Anna *et al.*, 2004; Jones & Renaut, 2010; Özkul *et al.*, 2013).

In the study area, this lithotype is characterized by a light brown to beige colour. Travertine fragments are usually 3 to 4 cm in diameter with the maximum being up to 20 cm (Fig. 2E), and the layers are 40 to 50 cm thick. The clasts are poorly sorted, angular to subrounded and slightly imbricated to the flow direction. The oxidation level can be observed in some parts and fragments are entombed in a muddy matrix. The fragments of this travertine lithotype are manifested as scour channel fill deposits settled in the top of the parallel laminated travertine bodies (Fig. 2G). Intraclast travertine lithotypes are widespread in all quarries (except Site-IV; Fig. 3).

Micritic travertine including gastropods (L6)
Small snails are common in the micritic travertines (Fig. 2F). The thickness of this lithotype varies in each section and ranges from 40 cm to 2 m. In addition, unidentified gastropod shells, ostracods, crab fragments and leaf fossils are very common in Site-IV.

Extra-formational pebbly travertine lithotypes (L7)
Pebbles are well-rounded, matrix-supported and mostly derived from ophiolitic rocks such as dunite, serpentinite and gabbro (Fig. 2H). In addition, these pebbles have been observed as channel-shape bodies in the travertine. This lithotype reaches a thickness of 50 cm and is clearly visible in the margin of Section-II.

Palaeosol (L8)
Palaeosols are observed as horizontal layers at different levels in all measured sections (Fig. 2B and G), ranging from 10 to 50 cm in thickness. They are dark brown to grey coloured, are rich in organic matter and have irregular bases. The palaeosols unconformably overlie the reed lithofacies (Figs 2G and 3). Lateral extensions of the palaeosol layers change from a few tens of metres up to a few hundred metres. Each palaeosol layer and associated erosional surface (Fig. 2) constitutes a sequence boundary between two different travertine beds; this level is locally enhanced by the presence of dark clays.

Depositional system and facies

The travertine depositional system corresponds to a specific environment that can be delineated based on the description of physical (grain size, components, erosional features and bedding), chemical (inorganic, dissolution and precipitate) and biological (microbial) imprints.

In this work, a single depositional system has been recognized; this system is subdivided into facies types composed of lithotype combinations. The investigated travertines precipitated from slowly flowing water and partly ponding spring waters in depressions that consist of 'Flat-Pool Facies', and 'Marsh-Pool Facies' like those in Rapolano Terme (Guo & Riding, 1998). In the study area, the Flat-Pool facies is characterized by laterally extensive light coloured parallel laminations and associated intercalations of the paper-thin rafts and coated bubbles, whereas the Marsh-Pool facies is observed as dark coloured in the field and mostly consists of

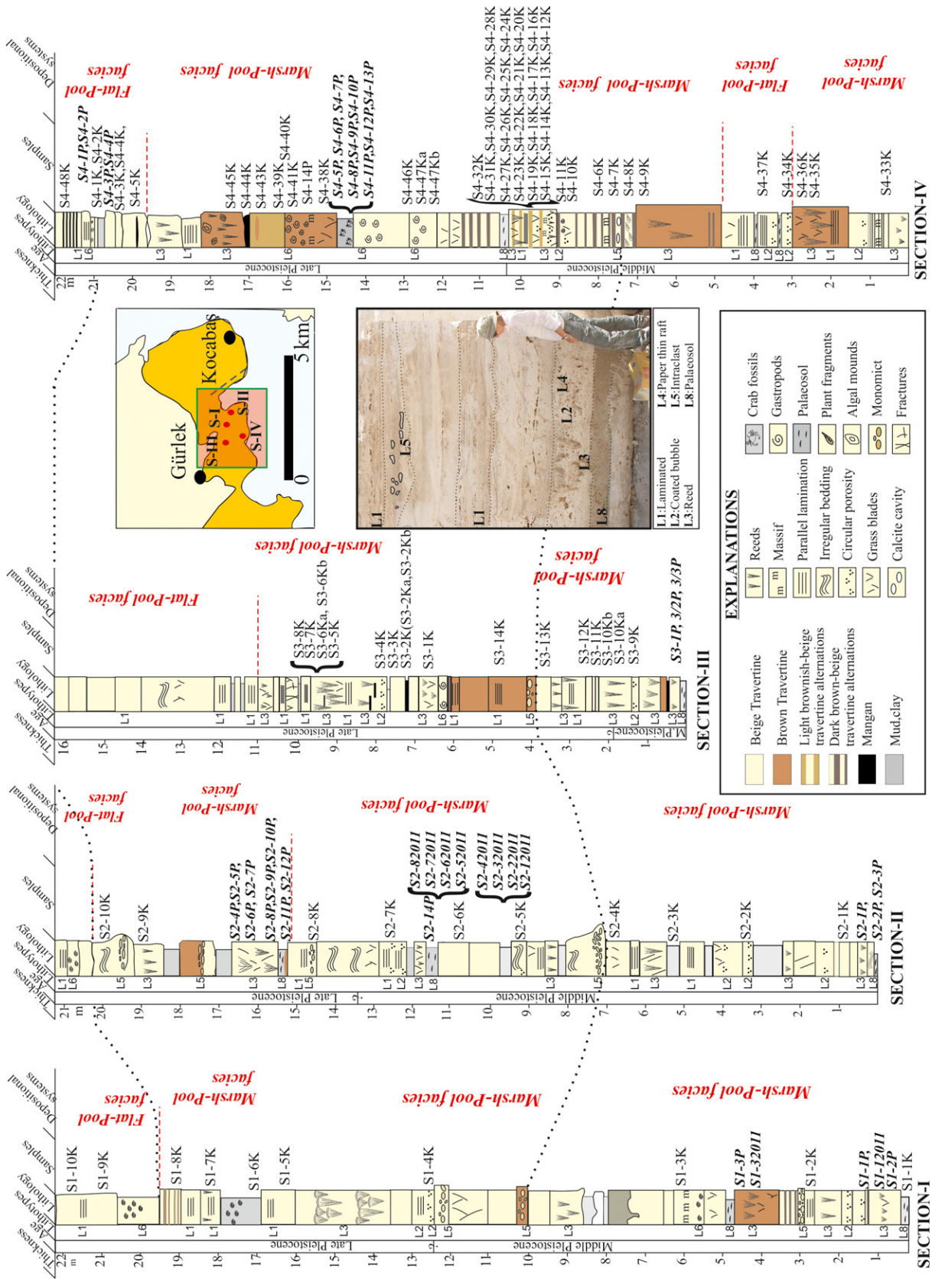

Fig. 3. Illustrated correlated sections, lithotypes and depositional systems of Kocabaş travertines.

intraclast and reed travertines. Both Flat-Pool and Marsh-Pool facies generally exhibit horizontal stratification, although in some cases they are cut by erosional levels containing muddy, silty materials.

Flat-Pool facies

Description. Flat-Pool facies has been used for light coloured horizontally thin-bedded travertine precipitations; it is characterized by parallel laminated (L1) lithotype. This facies is characterized by a *ca* 2 to 4 m thickness and tens to hundred metres in lateral extent through the all studied sections (Fig. 3).

Interpretation. Flat-Pool facies is formed in shallow ponds probably fed by subaqueous springs upwelling along the faults and fractures (Chafetz & Folk, 1984; Guo & Riding, 1998; Facenna *et al.*, 2008; Özkul *et al.*, 2013). Although the shrub lithotype is the most prominent component of the light coloured travertines precipitated in depressions (Chafetz & Folk, 1984; Guo & Riding, 1998; Facenna *et al.*, 2008), the Flat-Pool facies of the Kocabaş travertines lacks the shrub lithotype. However, other characteristics, such as horizontal bedding, parallel lamination, lateral extension of tens to hundred metres, light colour, palaeosols, mud and clay intercalations indicate Flat-Pool facies.

Marsh-Pool facies

Description. The term Marsh-Pool facies has been used by Guo & Riding (1998) for grey to brown coloured reed and lithoclast travertines (L3 and L5). In addition, gastropods and ostracods are locally common in this facies (L6 lithotype; Figs 2 and 3). Pedogenic effects are locally intense (Section-IV). Particularly, Marsh-Pool facies are interlayered with Flat-Pool facies and silty, muddy erosive levels.

Interpretation. These deposits form in shallow lake or pool environments; they accumulate in locations distal to warm springs, where water temperatures are lower due to mixing with cool

Table 1. Stable carbon and oxygen isotope results from the Kocabaş travertines.

Sample no	$\delta^{13}C$ (V-PDB)	$\delta^{18}O$ (V-PDB)	$\delta^{18}O$ (V-SMOW)	Sample no	$\delta^{13}C$ (V-PDB)	$\delta^{18}O$ (V-PDB)	$\delta^{18}O$ (V-SMOW)
S4-1K	1·8	−8·9	21·8	S4-31K	1·6	−8·6	22·1
S4-2K	1·7	−9·7	20·9	S4-32K	1·7	−8·1	22·5
S4-3K	1·4	−10·1	20·5	S4-33K	1·9	−9·3	21·3
S4-4K	1·3	−9·8	20·9	S4-34K	2·0	−9·5	21·1
S4-5K	1·4	−9·4	21·2	S4-35K	1·8	−8·7	22·0
S4-6K	2·2	−8·7	22·0	S4-36K	1·5	−8·7	21·9
S4-7K	1·9	−8·8	21·8	S4-37K	1·8	−8·0	22·6
S4-8K	1·9	−8·2	22·5	S4-38K	1·5	−10·5	20·1
S4-9K	1·8	−7·3	23·4	S4-39K	1·5	−10·1	20·5
S4-10K	1·9	−7·9	22·8	S4-40K	1·4	−10·1	20·5
S4-11K	1·7	−7·2	23·5	S4-41K	1·7	−10·2	20·4
S4-12K	1·9	−8·8	21·8	S4-43K	1·1	−10·4	20·2
S4-13K	1·6	−7·6	23·1	S4-44K	1·2	−10·4	20·2
S4-14K	1·3	−7·2	23·5	S4-45K	2·2	−9·1	21·5
S4-15K	2·2	−8·7	21·9	S3-1K	1·9	−7·6	23·1
S4-16K	1·9	−8·4	22·2	S3-2K/a	2·0	−9·5	21·1
S4-17K	1·9	−7·9	22·7	S3-2K/b	1·9	−9·2	21·5
S4-18K	1·8	−7·8	22·9	S3-3K	1·8	−9·1	21·6
S4-19K	1·8	−8·9	21·8	S3-4K	1·7	−8·1	22·5
S4-20K	1·9	−8·1	22·6	S3-5K	1·8	−7·2	23·5
S4-21K	1·9	−8·4	22·2	S3-K/a	2·0	−7·4	23·3
S422K	1·9	−8·1	22·6	S3-6K/b	1·7	−6·4	24·3
S4-23K	1·9	−7·8	22·9	S3-7K	1·7	−8·4	22·2
S4-24K	1·9	−9·5	21·1	S3-8K	1·6	−7·1	23·6
S4-25K	1·9	−8·2	22·4	S3-9K	2·6	−8·6	22·1
S4-26K	2·0	−9·2	21·5	S3-10K/a	2·6	−8·3	22·4
S4-27K	1·8	−8·1	22·6	S3-10K/b	2·6	−8·2	22·5
S4-28K	1·8	−8·7	21·9	S3-11K	2·5	−8·2	22·4
S4-29K	1·5	−8·4	22·2	S3-12K	2·2	−9·1	21·5
S4-30K	1·5	−8·7	21·9	S3-13K	2·5	−8·7	21·9

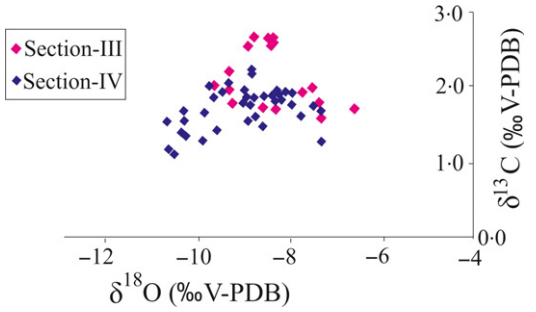

Fig. 4. Stable carbon versus oxygen isotopic cross-plot for Kocabaş travertines (Site-III and Site-IV). $\delta^{18}O$ values of Site-III varies between −9·5‰ and −6·4‰ whereas $\delta^{13}C$ values are between 1·6‰ and 2·6‰. $\delta^{18}O$ values of Site-IV range from −10·5 to −7·2‰ and $\delta^{13}C$ values from 1·1 to 2·2‰.

surface meteoric water. According to Guo & Riding (1998), stagnant lakes or pools fed by sulphur-rich springs display the greatest percentage of bacterially precipitated travertine (for example, H_2S-rich bath at Bagni di Tivoli). Even if this type of lake-fill travertine was not observed in the quarries, the depositional patterns on the quarry walls may indicate strong evidence for the Marsh-Pool facies.

Stable isotopic composition

The results of stable carbon and oxygen isotope analyses of the Kocabaş travertines are summarized in Table 1 and plotted in Fig. 4. According to these analyses, Kocabaş travertines have $\delta^{18}O$ values from −10·4 to −6·4‰ (VPDB) and have $\delta^{13}C$ values from 1·1 to 2·6‰ (VPDB) (Table 1).

Age determinations

The U/Th ages and isotopic ratios for 13 travertine samples are given in Table 2. The isotopic ratio of $^{230}Th/^{232}Th$ (standing for the degree of sample contamination) indicates the reliability of the final results; U/Th ages are considered reliable when $^{230}Th/^{232}Th$ is >17. However, if $^{230}Th/^{232}Th$ is <10, the obtained dates are considered less reliable, because they are probably showing contamination with older terrigenous material (Juliá & Bischoff, 1991).

The Kocabaş shallow lake-type travertine body (Site-II) yielded the oldest ages among the dated samples (*ca* 181·2 ± 7·7 ka), even though the $^{230}Th/^{232}Th$ ratios were <17. The travertine body (Site-IV) gave the youngest age (*ca* 85·5 ± 5·8 ka).

Palynological record and palaeovegetation

The results of palynological analyses of all studied sections are given below in detail. Spore species were not recorded; however, pollen species were observed abundantly and were less varied in palaeosol samples of Section-I, Section-II and Section-IV. The distribution of palynomorphs in these sections could be related to the lower humidity, the taphonomy, the lower diversity of plants, the transportation of pollen and spores (especially Gymnosperm pollen) and/or the changeable palaeoclimatic conditions.

Table 2. U/Th isotopic compositions and radiometric age data of travertine samples from Kocabaş. Samples with significant detrital contamination are related to $^{230}Th/^{232}Th<10$. This contamination, in general renders too old nominal dates calculated from $^{230}Th/^{234}U$. Six samples of lesser purity are related to $^{230}Th/^{232}Th<17$.

Sample	^{238}U (ppm)	^{232}Th (ppm)	$^{234}U/^{238}U$	$^{230}Th/^{234}U$	$^{230}Th/^{232}Th$	Ages (kyr)
S1-10K	0·3533	0·0045	1·2145 ± 0·008	0·6281 ± 0·004	184·5590 ± 1·16	103·7780 ± 1·4
S1-5K	0·1060	0·0180	1·2096 ± 0·009	0·8987 ± 0·007	197·4037 ± 2·10	Age calculated does not converge
S1-1K	0·1372	0·0037	1·2148 ± 0·007	0·8168 ± 0·007	113·8210 ± 1·09	169·3350 ± 3·8
S2-10K	0·3132	0·0877	1·2119 ± 0·007	0·6578 ± 0·006	8·6968 ± 0·09	104·0000 ± 3·9
S2-1K	0·0723	0·0169	1·2120 ± 0·008	0·8522 ± 0·009	13·5088 ± 0·10	181·2670 ± 7·7
S3-14K	0·1920	0·0100	1·3930 ± 0·010	0·6929 ± 0·010	54·2065 ± 0·50	118·3170 ± 3·0
S3-12K (b)	0·2157	0·0026	1·2184 ± 0·030	0·7058 ± 0·010	217·4143 ± 4·00	125·9506 ± 3·0
S4-39K	0·3764	0·2103	1·4626 ± 0·010	0·6097 ± 0·009	4·8774 ± 0·08	85·5120 ± 5·8
S4-41K	0·3450	0·0058	1·2473 ± 0·009	0·6440 ± 0·008	7·3117 ± 0·10	99·8650 ± 4·5
S4-38K	0·4051	0·1835	1·2585 ± 0·007	0·6764 ± 0·008	5·7433 ± 0·08	106·2170 ± 5·9
S4-32K	0·1282	0·0294	1·2400 ± 0·010	0·7377 ± 0·010	12·1999 ± 0·20	131·4930 ± 4·8
S4-20K	0·1461	0·0276	1·2263 ± 0·010	1·0696 ± 0·010	21·2362 ± 0·10	Age calculated does not converge
S4-15K	0·1109	0·0182	1·2263 ± 0·009	0·7474 ± 0·010	17·0234 ± 0·20	136·7820 ± 4·5

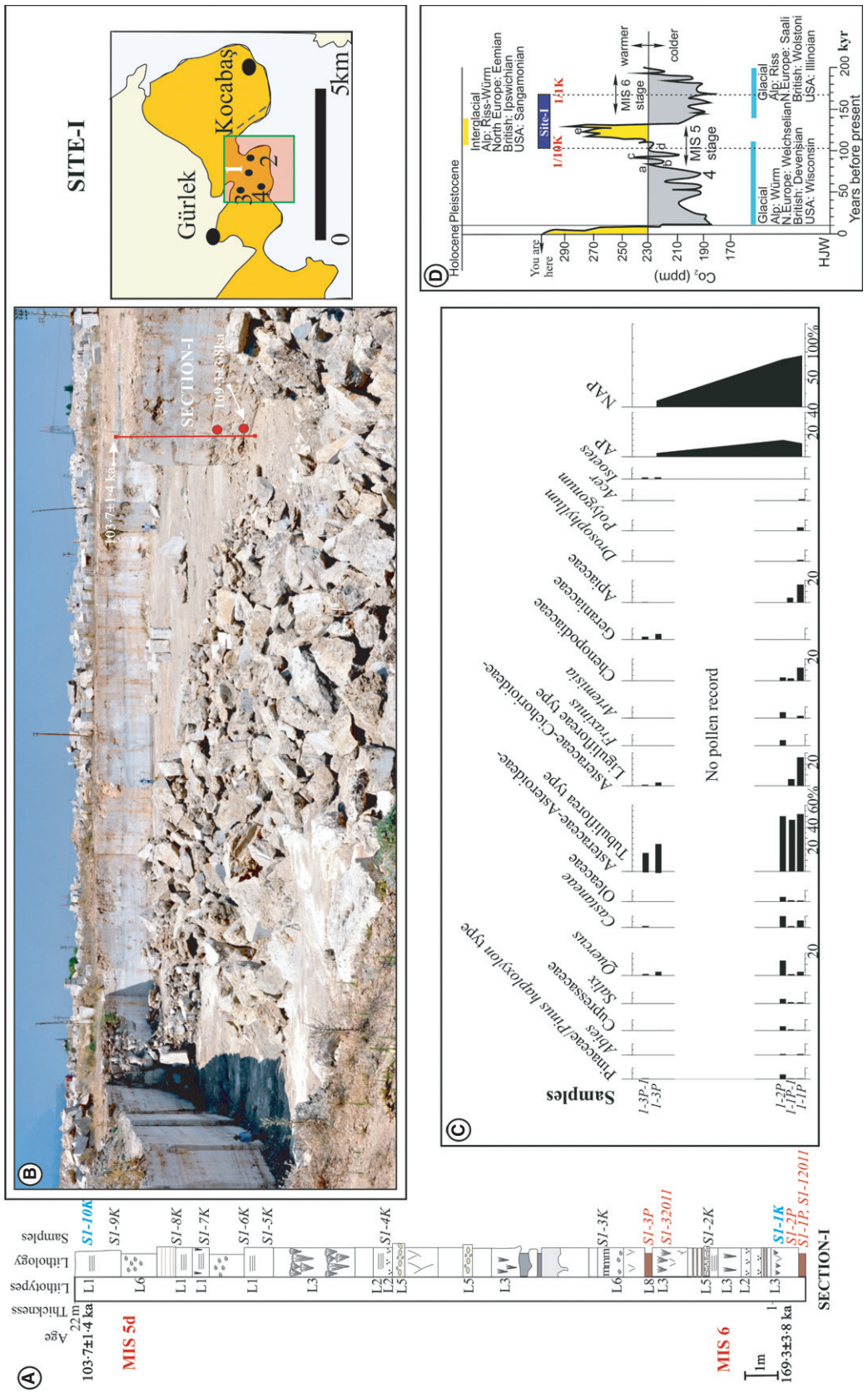

Fig. 5. (A) and (B) Measured stratigraphic section of Site-I and study area. (C) Pollen diagram of Site-I in the Kocabaş area. (D) Isotopic stages of the Late Pleistocene and Holocene.

Site-I

The palynological data were obtained from the palaeosol sediments (L8) in the lower part of the section of Site-I; these sediments should be older than the travertine level in which the S1-1K sample of 169 ka was collected (Fig. 5). Palynoflora is characterized by a high abundance of non-arboreal species (*ca* 90 to 95%). Asteraceae–Asteroideae and Asteraceae–Cichorioideae occur in high percentages in the palynospectra and also other palynomorphs accompanying aquatic and xerophytic herbaceous species (*Polygonum,* Geraniaceae, *Artemisia*, Chenopodiaceae, Apiaceae and *Isoetes*). The *Quercus* evergreen type is abundantly observed, whereas *Pinus*, *Abies*, *Salix*, *Castanea*, *Fraxinus* and Oleaceae of arboreal species are less abundant (Fig. 5C).

Site-II

Palynological records were obtained from three palaeosol levels (L8) of the stratigraphic Section-II in which three palynological groups were identified. In the lower part of the section, *Pinus*, Asteraceae–Asteroideae and *Fraxinus* were the most widely observed flora, yet were not abundant. The second palynoflora, from the middle part of the section, included Pinaceae (*Pinus* and *Abies*) and fewer amounts of grassland species (Asteraceae–Asteroideae and Chenopodiaceae) as well as other minor taxa (*Carpinus*, *Salix*, *Quercus*, Oleaceae and *Pterocarya*). According to previous studies, the high abundance of *Pinus* pollen were strongly related to altitudinal changes, latitudinal and longitudinal gradients, environmental setting, as well as transportation of pollen by water and/or wind (Markgraf, 1980; Jacobson & Bradshaw, 1981; Solomon & Silkworth, 1986; Sugita, 1993; Bertini *et al.*, 2014). However, the presence of *Abies* may indicate high topography near the deposition area (for example, Honaz Mountain) and/or climatic change. The third palynoflora was found in the upper part of the section [Marine Isotope Stage (MIS) 5e] and was comprised of Taxodioideae, *Quercus*, Oleaceae, grassland species (Centaureae, Poaceae and Asteraceae–Asteroideae) and the less abundant Pinaceae. Changes in the abundance of Pinaceae and grassland species and the presence and/or absence of the *Carpinus* and *Abies* could indicate a change in the palaeoclimatic conditions (Fig. 6A, B and C).

Site-III

Claystone and mudstone samples were collected from sediments at this site, however, palynomorph content was absent for the palynological interpretation (Fig. 7).

Site-IV

Eighteen claystone samples of the palaeosol levels were collected from the middle and upper part of Section-IV; palynological data were obtained from these samples. In the lower part of the section, leaf fossils possibly belonging to Fagaceae (cf. *Quercus*) and pollen of the grassland species were found.

The first palynological datum was recorded from 12 claystone samples of the palaeosol sediments located in the lower part of the S4-38K sample, although there is not a varied pollen content at this site. Palynoflora is represented by arboreal plants including Pinaceae (*Pinus* and *Abies*), *Quercus*, *Phillyrea* and Oleaceae. Ericaceae, Asteraceae–Asteroideae, and Chenopodiaceae are less abundant in the palynospectra. The second pollen record was obtained from the S4-1P-4P samples, and it is characterized by only grassland species (for example, Asteraceae–Cichorioideae and Asteroideae; Fig. 8).

DISCUSSION

Palaeoenvironmental reconstruction of the Kocabaş Basin

As clearly observed in the field, the measured sections of the Kocabaş travertines are laterally related to each other (Fig. 3). Some horizons of the travertine precipitation contain abundant gastropod remains that are a key tool for correlation of measured sections.

The travertines formed in a shallow lake or pool environment fed by thermal spring waters diluted by meteoric waters are comparable to travertine in localities such as Italy (Bagni di Tivoli – Chafetz & Folk, 1984; Minissale *et al.*, 2002; Facenna *et al.*, 2008; Rapolano Terme – Guo & Riding, 1998; Bertini *et al.*, 2008; Brogi & Capezzuoli, 2009; Brogi *et al.*, 2010) and Turkey (Ballık – Özkul *et al.*, 2002, 2013). Furthermore, the travertine depression deposition of Rapolano Terme consisted of two depositional systems, such as Shrub-Flat facies and Marsh-Pool facies. On the other hand, Bagni di Tivoli travertines contain Shrub facies, Terrace-Mound and Sloping-Mound facies (Guo & Riding, 1998; Brogi & Capezzuoli, 2009). The thickness of the travertine benches is similar across all sites. Kocabaş travertine started to precipitate earlier than Bagni di Tivoli travertines, according to the avail-

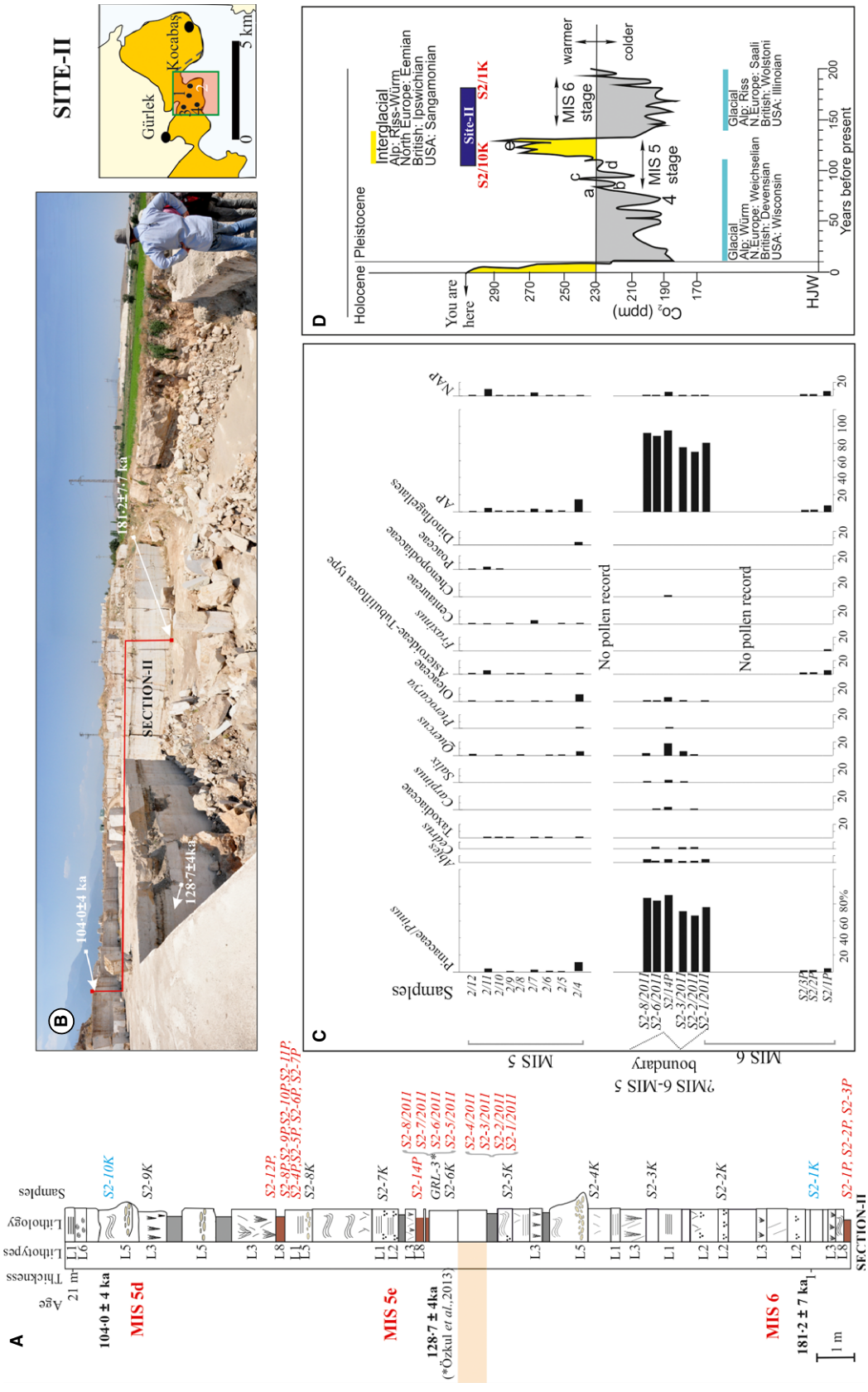

Fig. 6. (A) and (B) Measured stratigraphic section of Site-II and study area. (C) Pollen diagram of Site-II in the Kocabaş area. (D) Isotopic stages of the Late Pleistocene and Holocene.

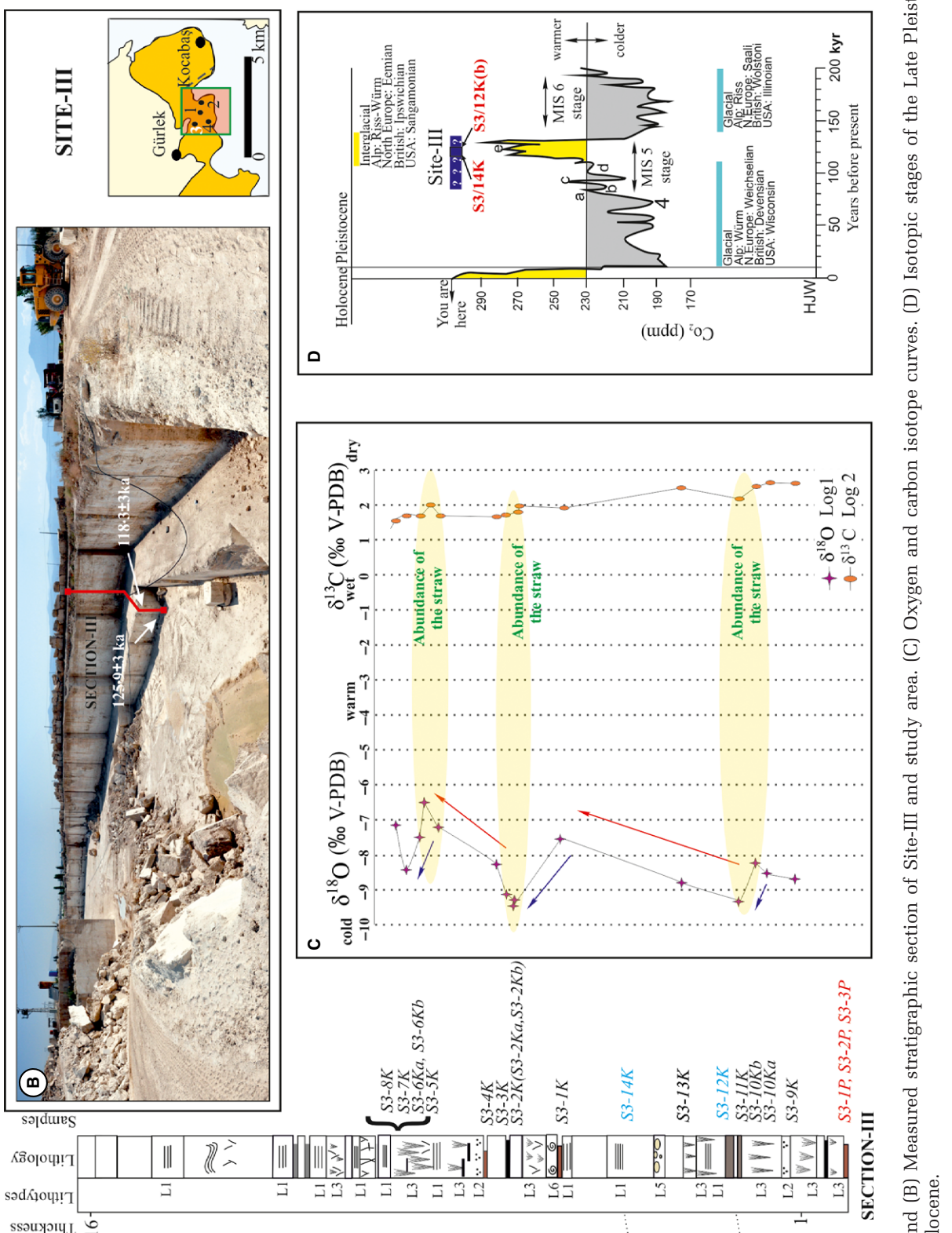

Fig. 7. (A) and (B) Measured stratigraphic section of Site-III and study area. (C) Oxygen and carbon isotope curves. (D) Isotopic stages of the Late Pleistocene and Holocene.

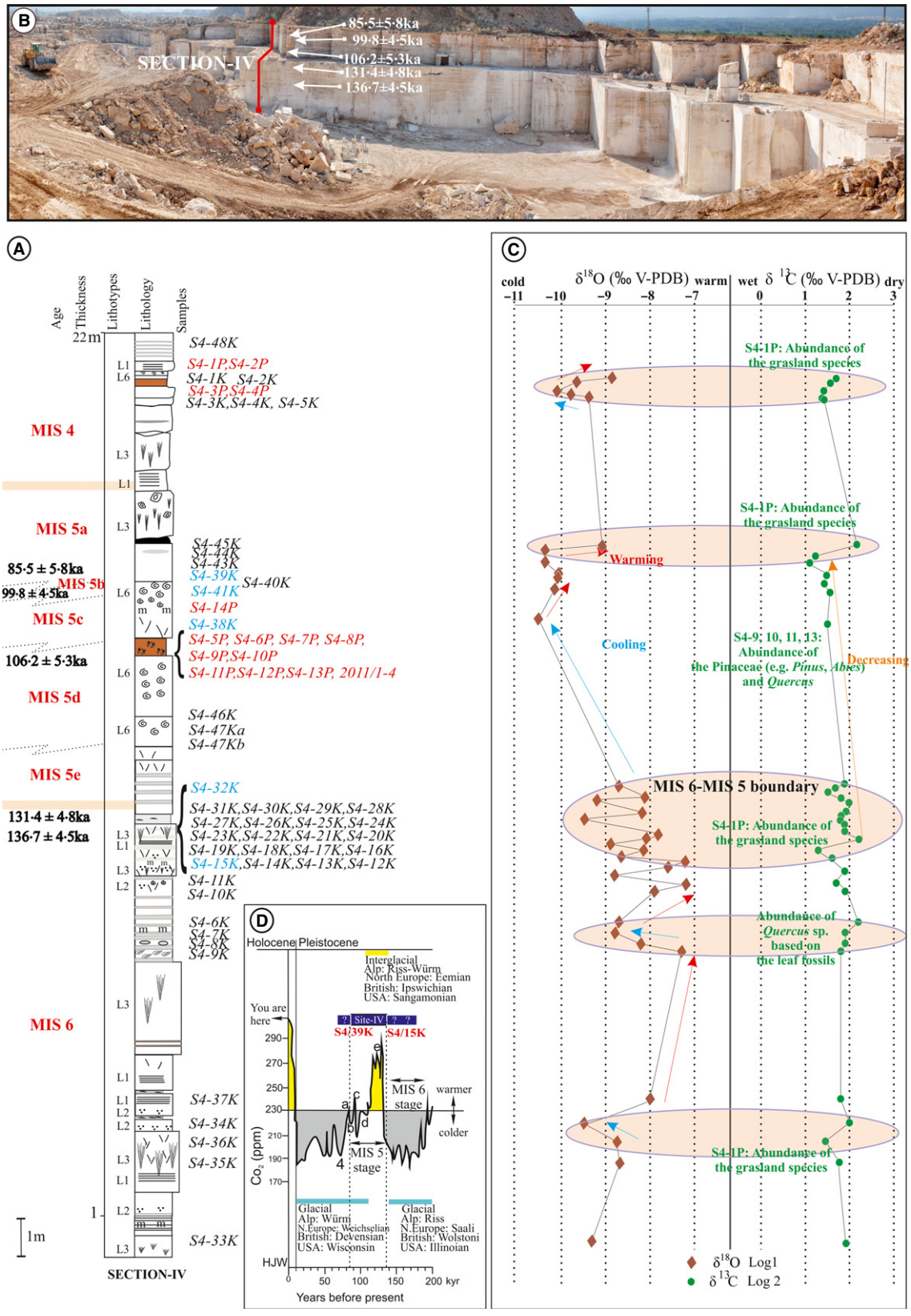

Fig. 8. (A) and (B) Measured stratigraphic section of Site-IV and study area. (C) Oxygen and carbon isotope curves with plant data. (D) Isotopic stages of the Middle to Late Pleistocene and Holocene.

Table 3. Comparison of the Kocabaş travertines with other shallow lake-fill type travertine deposits.

	Bagni Di Tivoli (Chafetz & Folk, 1984; Facenna *et al.*, 2008)	Rapolano Terme (Guo & Riding, 1998; Brogi & Capezzuoli, 2009; Brogi *et al.*, 2010)	Ballık (Özkul *et al.*, 2002, 2013)	Kocabaş travertines (this study)
Lithotype	Dominantly bacterial shrubs, layers of intraclasts, pockets of pisoids	Crystalline crust, shrub, pisoid, paper-thin raft, coated bubble, reed, litho-clast-breccia, palaeosol	Crystalline crust, shrub, pisolith, paper-thin raft, coated gas bubble, reed, lithoclast, pebbly travertine, palaeosol	Laminated, coated bubble, reeds, paper-thin raft, intra-clasts, gastropods, palaeosol
Facies	Shrub facies, Terrace-Mound facies, Sloping-Mound facies	Shrub-flat facies, marsh-pool facies	Pisolith, paper-thin rafts, coated gas bubble, reed, lithoclast, pebbly and palaeosols	Marsh-Pool facies, Flat-Pool facies
Fauna	Plethora (tiny oval bodies, *ca* 0·5 × 1·0 μm), blue-green algae, red and green algae, fungi	Ostracods, gastropods are locally common	Diatom, gastropods, bacterial filaments, irregular radial pisoliths (bacterially mediated)	Gastropods, crab fragments
Flora	Leaves, woody plants, shrubs, branches (stem or trunk)	Reeds	Reed, shrubs	Pollens (*Abies*, *Pinus*, *Quercus*, Compositae–Tubulifloreae)
Erosion surface	Five main erosional surfaces; palaeosols, conglomerates and karstic features	Clay-silt palaeosols	Solution cavities, microkarstic features	Palaeosols, karstic features
Lateral extension	200 to 300 m	Tens to hundreds of metres	Hundreds of metres	A few hundred metres
Thickness (m)	85	40	65	60
Age range (ka)	30 to 115	–	>500	80 to 181
Depositional environment	Shallow lake	Flats and hollows in areas of relatively low topography	Depression depositional (shrub-flat and marsh-pool subenvironments)	Depression depositional system like stagnant/low energy lake environment
Depositional process	Very shallow lake-fill deposits and terrigenous-rich layers are flood deposits into the lakes by severe storms	Precipitation from fast flowing spring water, low angle slopes, fine lithoclast shows pedogenic effects	Terrigenous materials are interpreted as floodings and ephemeral streams are associated with shrubs	Terrigenous materials can be explained by floodings, and hill-wash breccias are lower slope deposits into shallow lake

able dating results (Table 3). Lamination is a common sedimentary structure and it is usually interpreted as an effect of changes in water composition, temperature and biological activity in quiescent pools (Pentecost, 2005), and produced by the alternation and succession of different sized crystal laminae. Variations in density and colour are due to seasonal growth of algae or bacteria. The dark colour observed in the laminated levels correlates with high Fe and Mn oxide content. These horizontally bedded travertines can be interpreted as being deposited by slow and continuous laminar flows in depression fill. The coated bubbles associated with the paper-thin rafts observed in travertine bodies have occurred mostly where bubbles were trapped near pool surfaces below paper-thin rafts or vegetation in pools. On the other hand, thin rafts with gas bubbles imply rapid precipitation under stagnant conditions in a pool environment. Reeds are mainly an obstacle to water flow. Root structures stabilize the sediments and these plant materials become encrusted by fine-grained calcium carbonates, which fill the space (Guo & Riding, 1998). Furthermore, moulds of reeds, twigs, leaves and other plant structures hold on to the sediments because the water flow is obstructed during precipitation and afterwards they were covered by micritic carbonate. Reeds or plant materials are most probably responsible for the high porosity of the deposits; their organic matter content is much higher than in other travertine lithotypes. In general reed, grass and other plants grow away from the orifice of a hot spring, where the water is cool or diluted by rain. Gastropods are present at different parts of the travertine sequences indicating a lake-margin depositional environment. Rounded pebbles – including well-rounded grains of serpentinite, dunite and harzburjite – of a few centimetres in diameter in the studied travertines most probably derived from ephemeral flooding from nearby Neogene and pre-Neogene basement rocks (Özkul *et al.*, 2002). Unconsolidated materials were altered by exposure to rainwater, biological activities and subareal desiccations associated with soil formation (Guo & Riding, 1998).

Kocabaş depositional system model

The depositional model of the Kocabaş travertines is presented in Fig. 9 based on the information obtained from sedimentological evidence (for example, palaeosol, lamination, clasts, fauna and flora contents), stable isotopic results and dating. This model includes palaeoclimatic and palaeovegetational evolution of Kocabaş travertines from MIS 6 to 4. The studied sections can be correlated with one another based on this model and indicate that in the studied area the Kocabaş travertines were deposited in the same shallow lake environment. The gastropod levels and intraclast breccia levels also support this argument.

This model depicts the facies associations that resulted from initial extensional tectonic activity and faulting. Thermal water rich in dissolved carbonate came to the surface and deposited travertine on Neogene clastics such as sandstone, claystone and marl. Afterwards, the carbonate sedimentation spreads laterally to the related pool subenvironments. Figure 9A shows that travertine precipitation (Sites I, II, III and IV) started between 170 ka and 130 ka (glacial period) in one shallow pool environment. Palaeovegetation, mostly composed of straws and some herbs during the precipitation of palaeosols, and wooded areas that consisted of, for example *Abies*, *Pinus*, *Quercus* and Oleaceae, should have existed in the depositional environment.

During the last interglacial period (130 to 80 ka) travertine precipitation continued and the model presented in Fig. 9B corresponds to a stagnant pool environment where Flat-Pool and Marsh-Pool facies are prominent. The last model (Fig. 9C) corresponds to a glacial period MIS 4 (80 to 70 ka) showing that the travertine precipitation progressively moved to the north-west of the study area due to travertine deposition ceasing at Site-I and Site-II (Fig. 9C). This change possibly implies that local tectonic forces induced a spatial variation in the basin.

Palaeoclimatic implications

In general, travertine deposition can be correlated with both warm and cold climatic conditions (Pentecost, 1995; Frank *et al.*, 2000; Horvatincic *et al.*, 2005; Uysal *et al.*, 2009; Özkul *et al.*, 2013). The U–Th dating of horizontally bedded travertines of the Kocabaş area show that the travertines were deposited in MIS 5 represented by a humid/warm period, as well as MIS 4 and MIS 6 dry/cold periods (Shackleton *et al.*, 2003). The oxygen and carbon isotope records and palynomorph content also largely coincide with times of humid/warm and cold/dry climate events. According to some earlier studies, vein

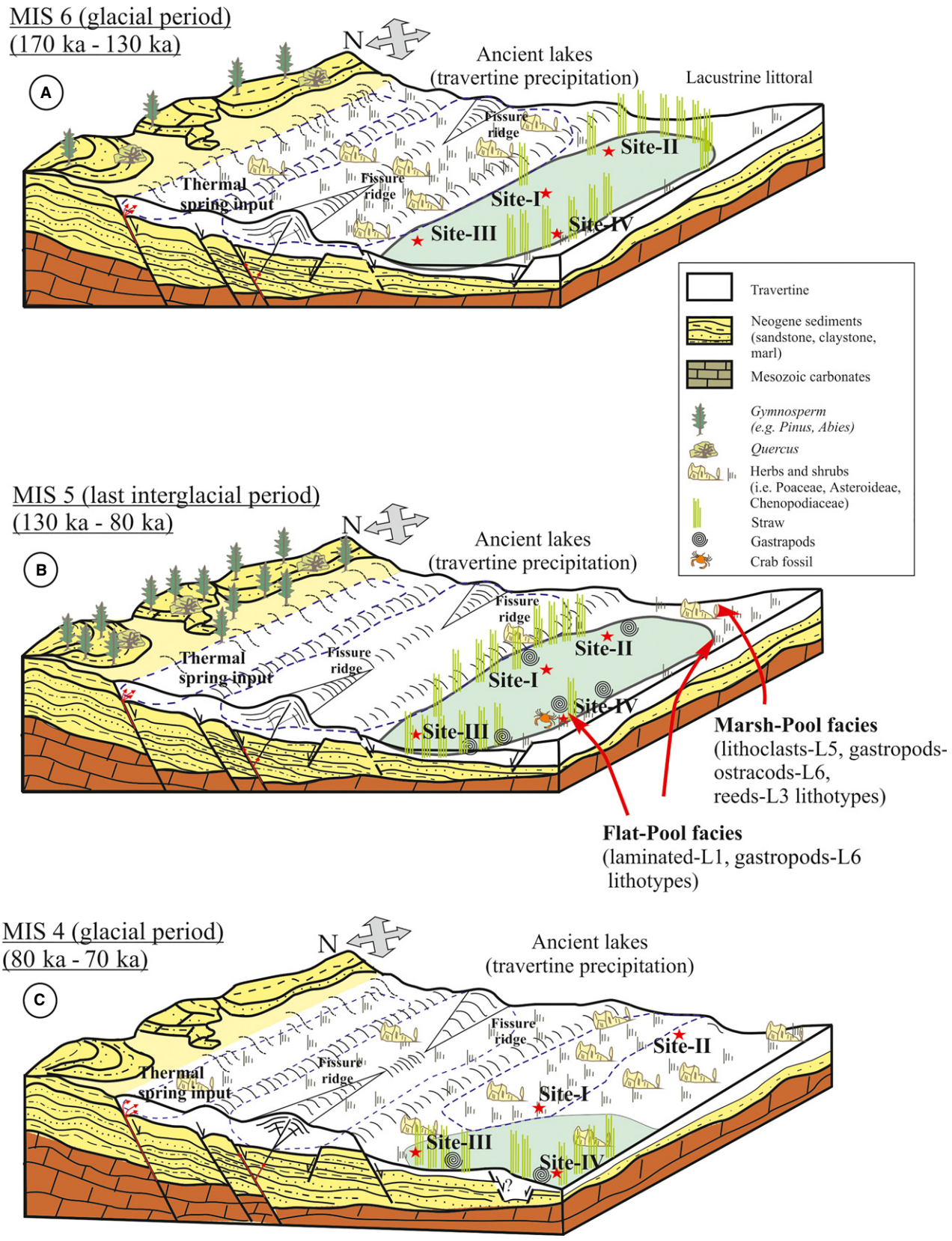

Fig. 9. Schematic block diagrams illustrating the palaeoenvironmental evolution of the Kocabaş (Gürlek) area during the Pleistocene. (A) The travertine precipitation in the lacustrine environment (including Site-I and Site-II sections) may have continued until MIS 5 (inter glacial period) according to the U/Th data. (B) Studied travertines were deposited on the Flat-Pool and Marsh-Pool facies. (C) At the same time, travertine depositional pools may have progressed to the south and continued until MIS 4 (glacial period).

travertines (cf. 'vertically banded travertines', Altunel & Hancock, 1993a) were attributed to dry/cold periods like MIS 2 and 4 (Uysal *et al.*, 2009; De Flippis *et al.*, 2012). However, travertine precipitation in the region has been continuous during warm and humid periods (for example, MIS 1, 3, 5 and 7) as well as cold and dry periods (for example, MIS 2, 4 and 6), irrespective of the type of travertine (Özkul *et al.*, 2013).

Pollen stratigraphy shows various vegetational phases, which can be distinguished on the basis of the AP–NAP (arboreal pollen and non-arboreal pollen) diagram. From 181 to 80 ka, several phases were recognized at each site and are described below.

According to the palynoflora of Site-I, which starts at 169·3 ± 4 ka (MIS 6; sample S1-1K) and ends at 103·7 ± 1 ka (MIS 5c; samples S1-10K), open vegetation was widespread throughout the site during the cold period of MIS 6 stage (Fig. 5). Abundance of the NAP percentage and xerophytic plant (Oleaceae and *Quercus* evergreen type) indicates drought in the cold climatic condition of MIS 6 (Fig. 5D). In addition, the presence of *Isoetes* displays summer dryness and wet winters (Botema & Sarpaki, 2003). Palaeosol deposition also coincides with the cold period of MIS 6 and it demonstrates a water level decrease possibly due to a wet winter or due to tectonic activity (Fig. 5C).

The deposition of Site-II started at 181·2 ± 7 ka (MIS 6; sample S2-1K) and ended 104·0 ± 3 ka (MIS 5d; sample S2-10K; Fig. 6). Furthermore, Özkul *et al.* (2013) obtained a date of deposition of 128·7 ± 3 ka (MIS 5e) at the same site (equivalent to samples S2-7-8K of this study; Fig. 6). Based on palynological data from this site, cooling at the end of MIS 6 stage is demonstrated by the abundance of Pinaceae-*Abies* during travertine deposition. The last palynoflora was taken from the upper part of Section-II and it is characterized by a decrease in Pinaceae and by a low percentage of the NAP (Asteroideae–Tubuliflorea, Centaureae and Poaceae). This floristic change could possibly indicate palaeoclimatic change, although there was probably no significant change in palaeotopography. The observed NAPs in the terrestrial area could be associated with the warm climatic conditions at the end of MIS 5e. The L5, L6 and L1 lithotypes are observed at the end of the stratigraphic section (MIS 5d; 104 ka) inferring increasing water levels in the pool. This environmental change in the lake could be related to a cooling phase in the MIS 5d stage, as seen at the top of Section-I at Site-I (Fig. 5).

According to the results of stable carbon and oxygen isotope analyses of the travertines from Site- III, in which 125·9 ± 3 ka and 118·3 ± 3 ka (MIS 5) age data were obtained from the S3-12K and S3-14K samples (Table 2), the $\delta^{13}C$ and $\delta^{18}O$ values range between +1·6‰ and +2·6‰ (VPDB) and between +21·1‰ and +24·3‰ (VSMOW), respectively (Table 2). There are three distinct decreasing trends in the $\delta^{18}O$ values, which can indicate cooling (Fig. 7). Particularly low $\delta^{18}O$ values were obtained from the travertine samples of the L1 and L2 lithotypes. Thus, palaeoclimate was cool during the deposition of laminated travertines. The L3 lithotype is indicative of a warming period, and consists of increased $\delta^{18}O$ and $\delta^{13}C$ values. In addition, this lithotype was typically composed of rich straw flora and gastropod fauna and thus represents shallow pool environmental conditions caused by warming.

Radiometric age data of S4-15K and S4-39K (136·7 ± 4 ka and 85·5 ± 5·8 ka, respectively) show intensive precipitation of travertine during MIS 6 to 4 (Fig. 8). Abundance of *Pinus* and *Abies* species could indicate cold climatic conditions; this interpretation at the end of MIS 5d of Site-IV is consistent with global climatic data (Adams *et al.*, 1999; Klotza *et al.*, 2003). The $\delta^{13}C$ values of the samples from S4-15K to S4-43K decrease, and this decline could possibly indicate wet climatic conditions during deposition, which would in turn explain the abundance of the Pinaceae. The second palynoflora defines the top of the stratigraphic section of palaeosols within Site-IV and it is represented only by grassland (for example, Asteroideae–Tubuliflorea type, Chenopodiaceae and Poaceae) species. Decrease in $\delta^{13}C$ values is supported by the abundance of AP pollen. There are five distinct changes in the $\delta^{18}O$ values in the stratigraphic Section-IV. The first change is seen in the early phase of MIS 6 in Section-IV. In this phase, a decrease in $\delta^{18}O$ values was observed,

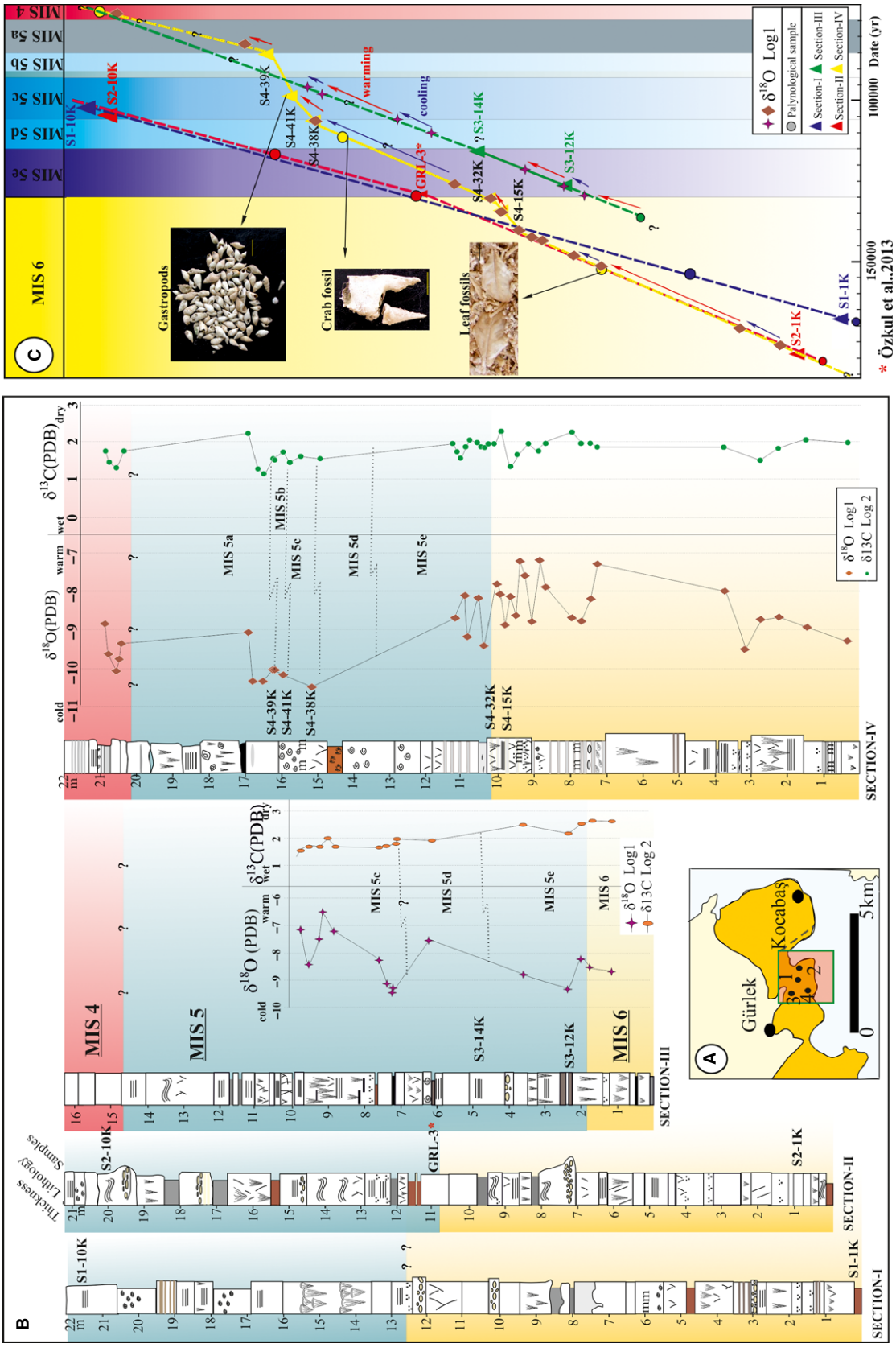

Fig. 10. Illustrated correlation chart of the facies, depositional time (U/Th dating) and stable isotopic curves of the study sites in the Kocabaş area. (A) Map of the study area and studied sections. (B) Measured stratigraphic sections of Kocabaş travertines and stable isotopic fluctuations. (C) Time frame for travertine precipitation (from MIS 6 to MIS 4) and indication of sampling points for stable isotope ($\delta^{18}O$ and $\delta^{13}C$) and palynological analyses.

indicating a cooling climate. The second change occurs at the upper part of MIS 6 and is represented by the increase in $\delta^{18}O$ values. This increase in $\delta^{18}O$ values indicates a warming climate. Throughout the MIS 6 and MIS 5 period the $\delta^{18}O$ values fluctuate, showing high values at the boundary. Complete samples from MIS 5e and MIS 5d phases could not be collected because the lithology was not suitable (the abundance of plant fragments) for isotopic study. These phases are represented by the L6 sedimentary lithotype. Although palaeoclimate change was recorded in MIS 5e, cooling was observed from MIS 5e to MIS 5c based on the decreasing $\delta^{18}O$ values. However, because of the lack of suitable samples between MIS 5e and MIS 5c, it is difficult to determine the precise time of climate change. Cooling in the study area could be matched to the global glacial period in MIS 5d (Shackleton *et al.*, 2003). Deposition during the MIS 5b stage is not significant. The MIS 5c and MIS 5a phases are characterized by fluctuations of the $\delta^{18}O$ values which could be related to the palaeoclimatic changes during MIS 5c to MIS 5a. The MIS 4 stage can be located in the upper part of the stratigraphic Section-IV, and during this stage both decreasing and increasing $\delta^{18}O$ values are recorded. This change could be explained by climatic fluctuations during MIS 4.

In conclusion, the Kocabaş travertines are a trustworthy recorder of warm and cold climatic intervals in a continental environment. Deposition during the MIS 5 phase was observed in all sections, whereas deposition in MIS 4 is recorded only in Section-III and Section-IV (Figs 5 and 7). Tectonic and palaeoclimatic effects may have had an important role in lake level changes and subsequently may have caused travertine deposition in Section-I and Section-II to cease before the MIS 4 phase (Figs 6, 7 and 10). Palaeoclimatic conditions at the end of MIS 6, MIS 5e and MIS 5d phases can be discerned and correlated based on the sedimentary facies and $\delta^{18}O$ values of the travertines. The MIS 5e period begins with warming and continues with cooling in both sections. The MIS 6 stage is generally represented by grassland species and straws in palaeosols of Section-I and Section-II. Based on the palynological data of Section-II and Section-IV, the lower part of the MIS 5 (MIS 5e and MIS 5d) stage is represented by Pinaceae, *Quercus*, Oleaceae and *Abies* (Fig. 10). Herbaceous plants were also found in this section, although in lower numbers.

CONCLUSIONS

1 Based on field observations, the travertine precipitation at Kocabaş area can be classified into eight lithotypes. These are laminated, coated bubble, reed, paper-thin raft, intraclasts, micritic travertine with gastropods, extra-formational pebbles and palaeosol layer (erosional horizon), respectively.

2 The studied travertines were mainly precipitated in a depressional depositional system, which is composed of Flat-Pool and Marsh-Pool facies.

3 Palynological analysis from palaeosol sediments shows the following. Site-I is characterized by a high abundance of non-arboreal species. The Asteraceae–Asteroideae–Tubuliflorea type and Asteraceae–Cichorioideae–Liguliflorea type of these species (and also other grassland species) were recorded in high percentages in the palynospectra. At Site-II the most notable plant belongs to Pinaceae (*Pinus* and *Abies*), which is abundant in the palynospectra, whereas grassland species (Asteroideae–Tubuliflorea and Chenopodiaceae) are rare at this site. Site-III was not suitable for palynological study, and Site-IV was mostly represented by leaf fossils, which may belong to *Quercus.* Site-IV also contained abundant Pinaceae (*Pinus* and *Abies*), *Quercus* and Oleaceae, as well as lower amounts of Ericaceae, Asteroideae–Tubuliflorea type, *Phyllirea* and Chenopodiaceae.

4 The $\delta^{13}C$ and $\delta^{18}O$ values range between 1·1 to 2·6‰ and −6·4 to −10·4‰, respectively, and can be correlated with the warm and cold periods of the marine $\delta^{18}O$ record between Marine Isotope Stage 6 and Marine Isotope Stage 4. Travertine deposition in the Kocabaş area occurred during Middle to Late Pleistocene time (i.e. between 181 ka and 80 ka) according to the U/Th dating and during a series of climate changes including glacial and interglacial intervals. These intervals can be referred to as warm Marine Isotope Stage 5 and cold Marine Isotope Stage 6 and Marine Isotope Stage 4. According to the radiometric dating, travertine precipitation started in the Middle to Late Pleistocene corresponding to the glacial and last interglacial periods in marine isotopic stages (MIS 6 and MIS 5).

5 Sedimentological analysis indicates that the Kocabaş travertines have been deposited in a shallow lake-fill or pool environment in the Middle to Late Pleistocene. Travertine precipitation started in a lacustrine environment during the Marine Isotope Stage 6 glacial period. Thick

travertine deposits formed during the last interglacial period Marine Isotope Stage 5. Travertine precipitation ended *ca* 103 ka in Site-I and Site-II, whereas precipitation at Site-III and Site-IV continued to accumulate until *ca* 80 ka. Active fault systems favoured the rise of deep waters that were discharged at the surface as hot springs and may have had an important role in this movement.

ACKNOWLEDGEMENTS

This work was supported financially by project 2010BSP005 of the Scientific Research Unit at Pamukkale University. The authors thank Bassam Ghalep for U/Th dating at the GEOTOP, University of Quebec, Montreal. The authors further thank Aydın Marble, Erdem Marble and Özçelik Marble for their logistical support at their travertine quarries. The authors are also thankful to Kaan Günerkan for his help during the fieldwork. Reviewers Enrico Capezzuoli and other anonymous reviewers are thanked for their valuable comments and for sharing their knowledge on travertine precipitation. The authors are grateful to Julian Andrews for kindly reading of manuscript and providing helpful comments. The authors also sincerely thank Erica Owens and Lisa Johnson for improving the English text as a native speaker. Special thanks also go to Tracy Frank and Daniel Ariztegui for editing the manuscript.

REFERENCES

Adams, J., **Maslin, M.** and **Thomas, E.** (1999) Sudden climate transition during the Quaternary. *Prog. Phys. Geogr.*, **23**, 1, 1–36.

Alçiçek, H., **Varol, B.** and **Özkul, M.** (2007) Sedimentary facies, depositional environments and palaeogeographic evolution of the Neogene Denizli Basin of SW Anatolia, Turkey. *Sed. Geol.*, **202**, 596–637.

Allen, E.T. and **Day, A.L.** (1935) *Hot Springs of Yellowstone National Park*. Carnegie Institute of Washington, Washington, DC, 466 pp.

Altunel, E. (1994) Active tectonics and the evolution of Quaternary travertines at Pamukkale, Western Turkey. PhD Thesis, Bristol University, UK [unpublished].

Altunel, E. and **Hancock, P.L.** (1993a) Morphology and structural setting of Quaternary Travertines at Pamukkale, Turkey. *Geol. J.*, **28**, 335–346.

Altunel, E. and **Hancock, P.L.** (1993b) Active fissuring and faulting in Quaternary travertines at Pamukkale, Western Turkey. *Z. Geomorphol. N.F*, **94**, 285–302.

Altunel, E. and **Karacabak, V.** (2005) Determination of horizontal extension from fissure ridge travertines: a case study from the Denizli Basin, Southwestern Turkey. *Geodin. Acta*, **18**, 333–342.

Andrews, J.E. (2006) Paleoclimatic records from stable isotopes in riverine tufas: synthesis and review. *Earth-Sci. Rev.*, **75**, 85–104.

Andrews, J.E., **Riding, R.** and **Dennis, P.F.** (1997) The stable isotope record of environmental and climatic signals in modern terrestrial microbial carbonates from Europe. *Palaeogeogr. Palaeoclimatol. Palaeoecol.*, **129**, 171–189.

Arenas, C., **Cabrera, L.** and **Ramos, E.** (2007) Sedimentology of tufa facies and continental microbialites from the Palaeogene of Mallorca Island (Spain). *Sed. Geol.*, **197**, 1–27.

Arenas, C., **Osa′car, C.**, **Sancho, C.**, **Va′zquez-Urbez, M.**, **Auque′, L.** and **Pardo, G.** (2010) Seasonal record from recent fluvial tufa deposits (Monasterio de Piedra, NE Spain): sedimentological and stable isotope data. In: *Tufas and Speleothems: Unravelling the Microbial and Physical Controls* (Eds M. Pedley and M. Rogerson), pp. 119–142. Geological Society, London.

Baker, G. and **Frostick, A.C.** (1951) Pisoliths, ooliths and calcareous growths in limestone caves at Port Campbell, Victoria. *J. Sed. Petrol.*, **21**, 85–104.

Bargar, K.E. (1978) Geology and thermal history of Mammoth Hot Springs, Yellowstone National Park, Wyoming. *U.S. Geol. Surv. Bull.*, **1444**, 55.

Bar-Matthews, M., **Ayalon, A.** and **Kaufman, A.S.O.** (1997) Late Quaternary paleoclimate in the Eastern Mediterranean Region from stable isotope analysis of speleothems At Soreq Cave, Israel. *Quatern. Res.*, **47**, 155–168.

Bertini, A., **Minissale, A.**, **Ricci, M.** and **Vaselli, O**. (2007) Pleistocene travertines of central Italy: paleoenvironmental reconstruction from pollen and stable isotopes. *GeoSed*, **2007**, 10.

Bertini, A., **Minissale, A.** and **Ricci, M.** (2008) Use of Quaternary travertines of central-southern Italy as archives of paleoclimate, paleohydrology and neotectonics. *Ital. J. Quatern. Sci.*, **21**, 99–112.

Bertini, A., **Minissale, A.** and **Ricci, M.** (2014) Palynological approach in upper Quaternary terrestrial carbonates of central Italy: anything but a 'mission impossible'. *Sedimentology*, **61**, 200–220.

Black, D.M. (1953) Aragonite rafts in Carlsbad Caverns, New Mexico. *Science*, **117**, 84–85.

Boch, R., **Spotl, C.**, **Reitner, J.M.** and **Kramers, J**. (2005) A lateglacial travertine deposit in Eastern Tyrol (Austria). *Austrian J. Earth Sci.*, **98**, 78–91.

Botema, S. and **Sarpaki, A.** (2003) Environmental change in Crete: a 9000-year record of Holocene vegetation history and the effect of the Santorini eruption. *Holocene*, **13**, 733–749.

Bozkurt, E. and **Oberhänsli, R.** (2001) Menderes Massif (Western Turkey): structural, metamorphic and magmatic evolution – a synthesis. *Int. J. Earth Sci.*, **89**, 679–708.

Brogi, A. and **Capezzuoli, E.** (2009) Travertine deposition and faulting: the fault related travertine fissure-ridge at Terme S. Giovanni, Rapolano, Terme (Italy). *Int. J. Earth Sci.*, **98**, 931–947.

Brogi, A., **Capezzuoli, E.**, **Aqué, R.**, **Branca, M.** and **Voltaggio, M.** (2010) Studying travertines for neotectonics investigations: Middle-Late Pleistocene syn-tectonic travertine deposition at Serre di Rapolano (Northern Apennines, Italy). *Int. J. Earth Sci.*, **99**, 1383–1398.

Brogi, A., **Capezzuoli, E.**, **Alçiçek, M.C.** and **Gandin, A**. (2014) Evolution of a fault-controlled fissure-ridge type

travertine deposit in the western Anatolia extensional province: the Çukurbag fissure-ridge (Pamukkale, Turkey). *J. Geol. Soc. London*, **171**, 425–441.

Çakır, Z. (1999) Along-strike discontinuities of active normal faults and its influence on Quaternary travertine deposition; examples from western Turkey. *Turk. J. Earth Sci.*, **8**, 67–80.

Capezzuoli, E. and **Gandin, A**. (2005) Facies distribution and microfacies of thermal-spring travertine from Tuscany. In: *Proceedings of the 1st International Symposium on Travertine* (Eds M. Özkul, S. Yagiz and B. Jones), pp. 43–49. Kozan Ofset Matbaacılık San. ve Tic. Ltd. Şti, Ankara.

Chafetz, H.S. and **Folk, R.L.** (1984) Travertines: depositional morphology and the bacterially constructed constituents. *J. Sed. Petrol.*, **54**(1), 289–316.

Chafetz, H.S., **Rush, P.F.** and **Utech, N.M.** (1991) Microenvironmental controls on mineralogy and habit of $CaCO_3$ precipitates: an example from an active travertine system. *Sedimentology*, **38**, 107–126.

De Flippis, L., **Facenna, C.**, **Billi, A.**, **Anzalone, E.**, **Brilli, M.**, **Özkul, M.**, **Soligo, M.**, **Tuccimei, P.** and **Villa, M.I.** (2012) Growth of fissure ridge travertines from geothermal springs of Denizli Basin, western Turkey. *Geol. Soc. Am.*, **124**, 1629–1645.

Dilsiz, C. (2006) Conceptual hydrodynamic model of the Pamukkale hydrothermal field, southwestern Turkey, based on hydrochemical and isotopic data. *Hydrogeol. J.*, **14**, 562–572.

Erdoğan, B. and **Güngör, T.** (2004) The problem of core-cover boundary of the Menderes Massif and an emplacement mechanism for regionally extensive gneissic granites, western Anatolia (Turkey). *Turk. J. Earth Sci.*, **13**, 15–36.

Facenna, C., **Soligo, M.**, **Billi, A.**, **Filippis, L.D.**, **Funiciello, R.**, **Rosetti, C.** and **Tuccimei, P.** (2008) Late Pleistocene depositional cycles of the Lapis Tiburtinus travertine (Tivoli, Central Italy): possible influence of climate and fault activity. *Global Planet. Change*, **63**, 299–308.

Fairchild, I.J., **Smith, C.L.**, **Baker, A.**, **Fuller, L.**, **Spötl, C.**, **Mattey, D.** and **Mcdermott, F**., and E.I.M.F. (2006) Modification and preservation of environmental signals in speleothems. *Earth Sci. Rev.*, **75**, 105–153.

Folk, R.L. (1993) SEM imaging of bacteria and nannobacteria in carbonate sediments and rocks. *J. Sed. Petrol.*, **63**, 990–999.

Folk, R.L., **Chafetz, H.S.** and **Tiezzi, P.A**. (1985) Bizarre forms of depositional and diagenetic calcite in hot spring travertines, central Italy. In: *Carbonate Cements* (Eds N. Schneidermann and P. Harris), *SEPM Spec. Publ.*, **36**, 349–369.

Frank, N., **Braum, M.**, **Hambach, U.**, **Mangini, A.** and **Wagner, G.** (2000) Warm period growth of travertine during the last interglaciation in southern Germany. *Quatern. Res.*, **54**, 38–48.

Gandin, A. and **Capezzuoli, E.** (2014) Travertine: distinctive depositional fabrics of carbonates from thermal spring systems. *Sedimentology*, **61**, 264–290.

Gündoğan, İ., **Helvacı, C.** and **Sözbilir, H.** (2008) Gypsiferous carbonates at Honaz Dağı (Denizli): first documentation of Triassic gypsum in western Turkey and its tectonic significance. *J. Asian Earth Sci.*, **32**, 49–65.

Guo, L. and **Riding, R.** (1998) Hot-spring travertine facies and sequences, Late Pleistocene Rapolano Terme, Italy. *Sedimentology*, **45**, 163–180.

Hancock, P.L., **Chalmers, R.M.L.**, **Altunel, E.** and **Çakir, Z.** (1999) Travitonics: using travertines in active fault studies. *J. Struct. Geol.*, **21**, 903–916.

Horvatincic, N., **Özkul, M.**, **Gökgöz, A.** and **Barešic, J**. (2005) Isotopic and geochemical investigation of tufa in Denizli province, Turkey. In: *Proceedings of 1st International Symposium on Travertine* (Eds M. Özkul, S. Yagiz and B. Jones), pp. 162–170. Kozan Ofset Matbaacılık San. ve Tic. Ltd. Şti, Ankara.

Jacobson, G.L., Jr and **Bradshaw, R.H.W.** (1981) The selection of sites for paleovegetational studies. *Quatern. Res.*, **16**, 80–96.

Jones, B. and **Renaut, R.W**. (2010) Calcareous spring deposits in continental settings. In: *Carbonates in Continental Settings: Facies, Environments, and Processes* (Eds A.M. Alonso Zarza and L.H. Taner), *Dev. Sedimentol.*, **61**, 177–204.

Juliá, R. and **Bischoff, J.L.** (1991) Radiometric dating of Quaternary deposits and the Hominid mandible of Lake Banyolas, Spain. *J. Archaeol. Sci.*, **18**, 707–722.

Kaiser, M.L. and **Asraf, R**. (1974) Gewinnung und praparation fossilee Pollen und Sporen sowie anderer Paynomorphae unter besonderer Berücksichtigung der siebmethode. *Geol. Jahrb.*, **A.25**, 85–114.

Kaymakçı, N. (2006) Kinematic development and paleostress analysis of the Denizli Basin (Western Turkey): implications of spatial variation of relative paleostress magnitudes and orientations. *J. Asian Earth Sci.*, **27**, 207–222.

Kazancı, N., **Boyraz, S.**, **Özkul, M.**, **Alçiçek, M.C.** and **Kadıoğlu, Y.K.** (2012) Late Holocene terrestrial tephra record at western Anatolia, Turkey: possible evidence of an explosive eruption outside Santorini in the eastern Mediterranean. *Global Planet. Change*, **80**, 36–50.

Kele, S., **Özkul, M.**, **Gökgöz, A.**, **Fórizs, I.**, **Baykara, M.O.**, **Alçiçek, M.C.** and **Németh, T.** (2011) Stable isotope geochemical and facies study of Pamukkale travertines: new evidences of low-temperature non-equilibrium calcite-water fractionation. *Sed. Geol.*, **238**, 191–212.

Kitano, Y. (1963) Geochemistry of calcareous deposits found in hot springs. *J. Earth Sci.*, University of Nagoya **11**, 68–100.

Klotza, S., **Guiotb, J.I.** and **Mosbruggera, V.** (2003) Continental European Eemian and early Würmian climate evolution: comparing signals using different quantitative reconstruction approaches based on pollen. *Global Planet. Change*, **36**, 277–294.

Koçyiğit, A. (2005) Denizli-graben horst system: basin fill, structure, deformational mode, throw amount and episodic evolutionary history, SW Turkey. *Geodin. Acta*, **18**, 167–208.

Ludwig, K.R. and **Paces, J.B.** (2002) Uranium-series dating of pedogenic silica and carbonate, Crater Flat, Nevada. *Geochim. Cosmochim. Acta*, **66**, 487–506.

Markgraf, V. (1980) Polle dispersal in a mountain area. *Grana*, **19**, 127–146.

Minissale, A., **Kerrick, D.M.**, **Magro, G.**, **Murrell, M.T.**, **Paladini, M.**, **Rihs, S.**, **Sturchio, N.C.**, **Tassi, F.** and **Vaselli, O.** (2002) Geochemistry of Quaternary travertines in the region north of Rome (Italy): structural, hydrologic and paleoclimatologic implications. *Earth Planet. Sci. Lett.*, **203**, 709–728.

Okay, A.I. (1989) Denizli'nin güneyinde Menderes masifi ve Likya naplarının jeolojisi (Geology of the Menderes Massif and the Lycian Nappes south of Denizli, Western Taurides). *Bull. Mineral Res. Explor.* (Maden Tetkik ve Arama, MTA), **109**, 37–51 (in Turkish).

Özkul, M., **Varol, B.** and **Alçiçek, M.C.** (2002) Depositional environments and petrography of Denizli travertines. *Bull. Mineral Res. Explor.*, **125**, 13–29.

Özkul, M., **Kele, S.**, **Gökgöz, A.**, **Shen, C.**, **Jones, B.**, **Baykara, M.O.**, **Fórizs, I.**, **Németh, T.**, **Chang, Y.** and **Alçiçek, M.C.** (2013) Comparison of the Quaternary travertine sites in the Denizli extensional basin on their depositional and geochemical data. *Sed. Geol.*, **294**, 179–204.

Özkul, M., **Gökgöz, A.**, **Kele, S.**, **Baykara, M.O.**, **Shen, C.-C.**, **Hançer, M.**, **Kaya, A.**, **Aratman, C.**, **Akın, T.** and **Örü, Z.** (2014) Sedimentological and geochemical characteristics of a fluvial travertine: a case from the eastern Mediterranean region. *Sedimentology*, **61**, 291–318.

Pedley, H.M. (2009) Tufas and travertines of the Mediterranean region: a testing ground for freshwater carbonate concepts and developments. *Sedimentology*, Special Volume, **56**, 221–246.

Pentecost, A. (1995) Quaternary travertine deposits of Europe and Asia Minor. *Quatern. Sci. Rev.*, **14**, 1005–1028.

Pentecost, A. (2005) *Travertine*. Springer-Verlag, Berlin, 445 pp.

Sant'Anna, L.G., **Riccomini, C.**, **Rodrigues-Francisco, B.H.**, **Sial, A.N.**, **Carvalho, M.D.** and **Moura, C.A.V.** (2004) The Paleocene travertine system of the Itaboraı′ basin, Southeastern Brazil. *J. S. Am. Earth Sci.*, **18**, 11–25.

Schreiber, B.C., **Smith, D.** and **Schreiber, E.** (1981) Spring peas from NewYork State: nucleation and growth of fresh water hollow ooliths and pisoliths. *J. Sed. Petrol.*, **51**, 1341–1346.

Shackleton, N.J., **Sánchez-Goñi, M.F.**, **Pailler, D.** and **Lancelot, Y.** (2003) Marine isotope substage 5e and the Eemian interglacial. *Global Planet. Change*, **36**, 151–155.

Şimşek, S., **Günay, G.**, **Elhatip, H.** and **Ekmekçi, M.** (2000) Environmental protection of geothermal waters and travertines at Pamukkale, Turkey. *Geothermics*, **29**, 557–572.

Solomon, A.M. and **Silkworth, A.B.** (1986) Spatial patterns of atmospheric polen transport in a montane region. *Quatern. Res.*, **25**, 150–162.

Sözbilir, H. (1997) Stratigraphy and Sedimentation of the Tertiary Sequences in the Northeastern Denizli Province (Southwest Turkey). University of Dokuz Eylul, PhD Thesis, 195.

Sözbilir, H. (2005) Oligo-Miocene extension in the Lycian orogen: evidence from the Lycian molasse basin, SW Turkey. *Geodin. Acta*, **18**, 255–282.

Spötl, C. and **Vennemann, T.W.** (2003) Continuous-flow IRMS analysis of carbonate minerals. *Rapid Commun. Mass Spectrom.*, **17**, 1004–1006.

Sugita, S. (1993) A model pollen source area for an entire lake surface. *Quatern. Res.*, **39**, 239–244.

Sun, R.S. (1990) Denizli-Usak Arasinin Jeolojisi ve Linyit Olanaklari [The geology of Denizli-Usak and lignite possibilities] Izmir, the report from MTA, No. 9985.

Uysal, I.T., **Feng, Y.**, **Zhao, J.**, **Işık, V.**, **Nuriel, P.** and **Golding, S.D.** (2009) Hydrothermal CO_2 degassing in seismically active zones during the late Quaternary. *Chem. Geol.*, **265**, 442–454.

Van Noten, K., **Claes, H.**, **Soete, J.**, **Foubert, A.**, **Özkul, M.** and **Swennen, R.** (2013) Fracture networks and strike-slip deformation along re-activated normal faults in Quaternary travertine deposits, Denizli Basin, western Turkey. *Tectonophysics*, **588**, 154–170.

Westaway, R. (1993) Neogene evolution of the Denizli region of western Turkey. *J. Struct. Geol.*, **15**, 37–53.

Westaway, R., **Guillou, H.**, **Yurtmen, S.**, **Demir, D.** and **Rowbotham, G.** (2005) Investigation of the condition at the start of the present phase of crustal extension in western Turkey, from observation in and around the Denizli region. *Geodin. Acta*, **18**, 313–342.

Manuscript received 11 February 2013; revision accepted 17 December 2014